The effect of strain rate on the viscoplastic behavior of isotactic polypropylene at finite strains

A.D. Drozdov and J. deC. Christiansen

Department of Production

Aalborg University

Fibigerstraede 16, DK–9220 Aalborg, Denmark

Abstract

Two series of uniaxial tensile tests are performed on isotactic polypropylene with the strain rates ranging from 5 to 200 mm/min. In the first series, injection-molded specimens are used without thermal pre-treatment. In the other series of experiments, the samples are annealed for 51 hour at 160 °C prior to testing.

A constitutive model is developed for the viscoplastic behavior of isotactic polypropylene at finite strains. A semicrystalline polymer is treated as an equivalent heterogeneous network of chains bridged by permanent junctions (physical cross-links and entanglements). The network is thought of as an ensemble of meso-regions connected with each other by links (lamellar blocks). In the sub-yield region of deformations, junctions between chains in meso-domains slide with respect to their reference positions (which reflects sliding of nodes in the amorphous phase and fine slip of lamellar blocks). Above the yield point, the sliding process is accompanied by displacements of meso-domains in the ensemble with respect to each other (which reflects coarse slip and fragmentation of lamellar blocks). To account for alignment of disintegrated lamellar blocks along the direction of maximal stresses (which is observed as strain-hardening of specimens in the post-yield region of deformations) elastic moduli are assumed to depend on the principal invariants of the right Cauchy–Green tensor for the viscoplastic flow.

Stress–strain relations for a semicrystalline polymer are derived by using the laws of thermodynamics. The constitutive equations are determined by 5 adjustable parameters that are found by matching observations. Fair agreement is demonstrated between the experimental data and the results of numerical simulation. A noticeable difference is revealed between the mechanical responses of non-annealed and annealed specimens: (i) necking of samples not subjected to thermal treatment precedes coarse slip and fragmentation of lamellar blocks, whereas cold-drawing of annealed specimens up to a longitudinal strain of 80% does not induce spatial heterogeneity of their deformation; (ii) the elastic modulus increases with the strain rate for non-annealed specimens and decreases for annealed samples.

Key-words: Isotactic polypropylene, Viscoplasticity, Annealing

1 Introduction

This paper is concerned with the influence of strain rate on the viscoplastic response of isotactic polypropylene (iPP) at isothermal loading with finite strains. The viscoplastic flow in semicrystalline polymers, polyethylene [1, 2, 3, 4, 5, 6, 7, 8, 9], polypropylene [10, 11, 12, 13, 14, 15, 16, 17, 18, 19, 20, 21, 22] and poly(ethylene terephthalate) [23, 24, 25, 26, 27, 28, 29, 30], has been a focus of attention in the past decade, which may be explained by the importance of the yielding phenomenon for the analysis of fiber- and film-drawing processes.

Injection-molded isotactic polypropylene is chosen for the experimental analysis for two reasons:

1. Polypropylene is widely used in industrial applications (ranged from oriented films for packaging to nonwoven fabrics and reinforcing fibres).

2. Injection-moded iPP is a semicrystalline polymer with a rather complicated crystalline morphology that is strongly affected by annealing [11, 12, 31, 32, 33, 34, 35, 36] and mechanical loading [10, 16, 18, 21, 22].

Isotactic polypropylene contains three basic crystallographic forms [35]: monoclinic α crystallites, (pseudo) hexagonal β structures, orthorhombic γ polymorphs, and "smectic" mesophase (arrays of chains with a better order in the longitudinal than in transverse chain direction). At rapid cooling of the melt (which is typical of the injection-molding process), α crystallites and smectic mesophase are mainly developed, whereas β and γ polymorphs are observed as minority components [31]. The characteristic size of α spherulites in an injection-molded specimen is estimated as 100 to 200 μm [16, 31]. These structures are formed by lamellae stacks with lamellar thicknesses ranging from 10 to 20 nm [16, 34] A unique feature of the crystalline morphology of iPP is the lamellar cross-hatching: development of transverse lamellae oriented in the direction perpendicular to the direction of radial lamellae in spherulites [35].

Transmission electron microscopy [32, 34] and polirized optical microscopy [32] reveal that annealing of iPP in the sub-melting interval of temperatures results in

- a decrease in the concentration of transverse lamellae (and disappearance of cross-hatching after thermal treatment above 150 °C),

- an increase in the fraction of ordered α crystallites (where helices in monoclinic unit cells are oriented in the same direction).

WAXS (wide-angle X-ray scattering) measurements [34, 36] demonstrate that annealing of isotactic polypropylene in the vicinity of a critical temperature $T_c \approx 157$ to 159 °C induces a second-order phase transition in which the ordered α phase is replaced by a new crystalline form with a larger lattice volume and a higher mobility of chains. As molecular mobility plays the key role in the viscoplastic behavior of semicrystalline polymers, one can expect that this transformation strongly affects the response of iPP. To study this phenomenon in detail, two series of uniaxial tensile tests are performed: (i) on specimens not subjected to thermal treatment, and (ii) on samples annealed for two days at 160 °C prior to loading.

Recent studies on mechanically-induced transformations of the crystalline structure of iPP [10, 16, 18, 21, 22] show that loading a specimen in the sub-yield region of deformations results in (i) inter-lamellar separation, (ii) rotation and twist of lamellae, (iii) fine slip of lamellar blocks (homogeneous shear of layer-like crystalline structures) [2, 4, 18], (iv) chain slip through the crystals [19], (v) sliding of tie chains along and their detachment from lamellar blocks [19], and (vi) activation of the rigid amorphous fraction (part of the amorphous phase located in regions surrounded by radial and transverse lamellae). Straining of isotactic polypropylene in the post-yield region of deformations induces (i) coarse slip of lamellar blocks (heterogeneous inter-lamellar sliding) and their fragmentation, (ii) detachment of chain folds and loops from surfaces of crystal blocks, (iii) disintergation of crystalline lamellae into a mosaic structure, and (iv) alignment of broken lamellar blocks along the direction of maximal stresses and formation of a fibrillar texture [2].

To develop a constitutive model for the mechanical response of a semicrystalline polymer, we apply a method of homogenization. According to this approach [7], a complicated micro-structure of isotactic polypropylene is replaced by an equivalent phase whose response captures essential features of the mechanical behavior of the semicrystalline polymer. An amorphous phase (treated as a network of macromolecules bridged by junctions) is chosen as the equivalent phase for the following reasons:

1. The viscoplastic flow in semicrystalline polymers is "initiated in the amorphous phase before transitioning into the crystalline phase" [6].

2. Sliding of tie chains along and their detachment from lamellae play the key role in the yielding phenomenon [19].

A semicrystalline polymer is thought of as an equivalent network of chains bridged by junctions (entanglements, physical cross-links on the surfaces of crystallites and lamellar blocks):

- To simplify the analysis, the network is treated as incompressible (observations show that the degree of compressibility of polypropylene is rather low: the growth of the tensile strain up to 8% causes an increase in the volume strain by less than 1% [37]). The hypothesis regarding incompressibility of semicrystalline polymers at large deformations has been previously applied to the analysis of the mechanical response of polyethylene [7, 9], polypropylene [15, 17] and poly(ethylene terephthalate) [23, 25].

- To exclude from the consideration viscoelastic effects (associated with rearrangement of chains), all nodes are treated as permanent (active strands cannot separate from junctions and dangling strands cannot merge with the network during the experimental time-scale).

- To describe the viscoplastic flow, the network is assumed to deform non-affinely (junctions can slide with respect to their reference positions under loading).

Unlike conventional theories of non-affine networks, two sliding processes are introduced. The first reflects motion of nodes in amorphous regions and fine slip of crystallites. This process is assumed to occur at any intensity of strains. The other is attributed to coarse slip

and fragmentation of lamellar blocks and it takes place in the post-yield region of deformations only. The difference between these two types of non-affine deformation is that sliding of junctions in amorphous domains does not produce dissipation of energy, whereas coarse slip and disintegration of lamellae result in a noticeable entropy production. At uniaxial tension, the yield point is associated with the elongation ratio, at which fragmentation of lamellar blocks starts.

The objective of this study is two-fold:

1. To report experimental data in two series of uniaxial tensile tests on injection-molded iPP specimens: the samples in the first series of tests were not subjected to thermal treatment, whereas those in the other series of experiments were annealed at 160 °C prior to loading.

2. To develop constitutive equations for the viscoplastic behavior of a semicrystalline polymer at finite strains and to determine adjustable parameters in the stress–strain relations by fitting observations in tensile tests with the strain rates ranging from $1.5 \cdot 10^{-3}$ to $6.2 \cdot 10^{-2}$ s^{-1} (practically in the entire region of cross-head speeds employed in conventional quasi-static tests).

Our goal is to assess the influence of thermal pre-treatment and strain rate on the viscoplastic response of isotactic polypropylene.

The exposition is organized as follows. Experimental data in uniaxial tensile tests are reported in Section 2. Kinematic relations for sliding of junctions are developed in Section 3. Kinetic equations for the rate-of-strain tensor (that describes sliding of junctions in amorphous regions and fine slip of lamellar blocks) are introduced in Section 4. Strain energy density of a semicrystalline polymer is calculated in Section 5. Constitutive equations for an isothermal deformation with finite strains and kinetic relations for coarse slip and fragmentation of lamellar blocks are derived in Section 6 by using the laws of thermodynamics. Phenomenological expressions for material functions are proposed in Section 7. The governing equations are simplified for uniaxial tension of an incompressible medium in Section 8. Adjustable parameters in the stress–strain relations are determined in Section 9 by matching the experimental data. The effect of strain rate on material parameters is discussed in Section 10. Some concluding remarks are formulated in Section 11.

2   Experimental procedure

Isotactic polypropylene (Novolen 1100L) was supplied by BASF (Targor). ASTM dumbbell specimens were injection molded with length 148 mm, width 10 mm and thickness 3.8 mm. Uniaxial tensile tests were performed at room temperature on a testing machine Instron–5568 equipped with electro-mechanical sensors for the control of longitudinal strains in the active zone of samples. The tensile force was measured by a standard load cell. The engineering stress, σ, was determined as the ratio of the axial force to the cross-sectional area of stress-free specimens. The true longitudinal stress, Σ, was calculated by means of the incompressibility condition as

$$\Sigma = \sigma k,$$

where k is the elongation ratio.

Two series of mechanical tests were carried out. Every test was performed on a new specimen.

The first series of experiments consisted of 7 tests on specimens that were not subjected to thermal treatment with the cross-head speeds 5, 10, 25, 50, 100, 150 and 200 mm/min (which correspond to the Hencky strain rates $1.54 \cdot 10^{-3}$, $3.02 \cdot 10^{-3}$, $7.22 \cdot 10^{-3}$, $1.49 \cdot 10^{-2}$, $3.09 \cdot 10^{-2}$, $4.56 \cdot 10^{-2}$ and $6.23 \cdot 10^{-2}$ s^{-1}, respectively). The specimens were elongated up to the Hencky strain $\epsilon_{\rm H} = 0.3$ that noticeably exceeded the strain corresponding to the onset of necking at all cross-head speeds. The chosen strain rates ensured nearly isothermal experimental conditions, on the one hand, and they allowed the viscoelastic effects to be neglected, on the other. The duration of tensile tests before necking of samples varied from 4 s for the highest cross-head speed to 180 s for the lowest one. Our recent study demonstrated that the amount of stress relaxing during this period did not exceed 10% [38].

The other series of experiments was performed on specimens that were annealed in an oven for 51 h at 160 °C and cooled by air. To minimize the effect of physical aging, mechanical tests were carried out one day after thermal treatment. The series consisted of 7 tests that were carried out with the same cross-head speeds as the experiments on non-annealed samples. The specimens were stretched up to the maximal Hencky strain, $\epsilon_{\rm H} = 0.6$. No necking of samples was observed in all experiments, except for the test with the maximal strain rate, $\dot{\epsilon}_{\rm H} = 6.23 \cdot 10^{-2}$ s^{-1}, where the onset of a weak neck was revealed at the elongation ratio $k \approx 1.75$.

The true longitudinal stress, Σ, is plotted versus the elongation ratio, k, in Figures 1 to 7 for the non-annealed specimens (only the experimental data below the necking points are presented) and in Figures 8 to 14 for the samples subjected to thermal pre-treatment.

A noticeable difference is observed between the engineering stress–engineering strain curves for non-annealed and annealed specimens.

A typical stress–strain diagram for a sample that was not subjected to thermal treatment demonstrates an increase in the engineering stress with the engineering strain below some strain $\epsilon_{\rm y}$ (close to the yield strain, $\epsilon_{\rm y}^{\circ} = 0.13$, provided by the supplier) and a very weak decrease (practically a horizontal plateau) in an interval between $\epsilon_{\rm y}$ and a strain, $\epsilon_{\rm n}$, at which a neck is formed. The presence of a rather wide region of maxima on the engineering stress–engineering strain curve does not allow the yield stress and the yield strain for a non-annealed specimen to be determined with a high level of accuracy (in agreement with the conventional approach in viscoplasticity of solid polymers [39], the yield point is associated here with the point of maximum on the engineering stress–engineering strain diagram). This situation is rather typical for semicrystalline polymers that are not subjected to thermal treatment prior to mechanical testing: a similar observation was reported in [23] for poly(ethylene terephthalate).

A stress–strain curve for an annealed sample reveals an increase in the engineering stress below the yield points, a sharp maximum on the engineering stress–engineering strain diagram, and a monotonical decrease in the engineering stress in the post-yield region of deformations. The true stresses, $\Sigma_{\rm y}$, corresponding to the points of maxima on the engineering stress–engineering strain curves, as well as the appropriate elongation ratios, $k_{\rm y}$, are plotted in Figure 15 versus the Hencky strain rate, $\dot{\epsilon}_{\rm H}$. This figure shows that the true yield stress, $\Sigma_{\rm y}$, monotonically increases with $\dot{\epsilon}_{\rm H}$, while the elongation ratio for yielding, $k_{\rm y}$,

is practically independent of the strain rate. It is worth noting that the yield strains for non-annealed specimens, ϵ_y, exceed the engineering yield strains, $\epsilon_y = k_y - 1$, for annealed specimens by a factor of 2 to 3.

The experimental data depicted in Figure 15 are fitted by the conventional equation (that can be developed within the concept of thermal activation of screw dislocations [3])

$$\Sigma_y = \Sigma_0 + \Sigma_1 \log \dot{\epsilon}_H, \tag{1}$$

where $\log = \log_{10}$ and the adjustable parameters Σ_m $(m = 0, 1)$ are determined by the least-squares technique. Figure 15 demonstrates fair agreement between the observations and their approximation by Eq. (1). It should, however, be noted that the area of applicability of the phenomenological relation (1) is rather narrow: it cannot be employed at very low strain rates (when the viscoelastic effects become important) and at high rates of straining (when rate-induced fracture mechanisms are dominant).

Our purpose now is to derive constitutive equations for the viscoplastic behavior of a semicrystalline polymer that can correctly match the experimental data plotted in Figures 1 to 14.

3 Kinematics of sliding

Denote by $\mathbf{r}_0$ the radius vector of an arbitrary point in the initial state (before external loads are applied) and by $\mathbf{r}(t)$ its radius vector in the deformed state at time $t \geq 0$. Transition from the initial state of a network to its actual state is determined by the deformation gradient

$$\mathbf{F}(t) = \frac{\partial \mathbf{r}(t)}{\partial \mathbf{r}_0}. \tag{2}$$

Sliding of junctions in the network with respect to their initial positions is treated as a transformation of the reference state, when a point with the initial radius vector $\mathbf{r}_0$ moves to the point with a radius vector $\mathbf{r}_s(t)$. This transformation is described by the deformation gradient

$$\mathbf{F}_s(t) = \frac{\partial \mathbf{r}_s(t)}{\partial \mathbf{r}_0}.$$

It is worth noting that a smooth mapping, $\mathbf{r}_s(t, \mathbf{r}_0)$, is determined only locally, which means that the new (intermidiate) configuration is not necessary Euclidean [40].

A semicrystalline polymer is modelled as an incompressible medium, which implies that its deformation from the reference state to the deformed state is isochoric (volume-preserving). We suppose that transformation of the initial reference state into the new reference state (characterized by the deformation gradient $\mathbf{F}_s$) is volume-preserving as well.

Transformation of the new reference state into the deformed state is determined by the deformation gradient

$$\mathbf{F}_e(t) = \frac{\partial \mathbf{r}(t)}{\partial \mathbf{r}_s(t)}.$$

The subscript indices "s" and "e" indicate that appropriate deformation gradients describe sliding of junctions and elastic deformation (the latter means that the strain energy density is a function of $\mathbf{F}_e$).

According to the chain rule for differentiation, the tensors $\mathbf{F}(t)$, $\mathbf{F}_s(t)$ and $\mathbf{F}_e(t)$ are connected by the relationship

$$\mathbf{F}(t) = \mathbf{F}_e(t) \cdot \mathbf{F}_s(t), \tag{3}$$

where the dot stands for inner product. Formula (3) coincides with the multiplicative presentation of the deformation gradient proposed in [23], where $\mathbf{F}_e$ is called the "network stretch" tensor and $\mathbf{F}_s$ is referred to as the "slippage stretch" tensor.

Differentiation of Eq. (2) with respect to time implies that

$$\frac{d\mathbf{F}}{dt}(t) = \frac{\partial \mathbf{v}(t)}{\partial \mathbf{r}(t)} \cdot \frac{\partial \mathbf{r}(t)}{\partial \mathbf{r}_0},$$

where $\mathbf{v}(t) = d\mathbf{r}(t)/dt$ is the velocity vector. Introducing the velocity gradient

$$\mathbf{L}(t) = \frac{\partial \mathbf{v}(t)}{\partial \mathbf{r}(t)},$$

and using Eq. (2), we obtain

$$\frac{d\mathbf{F}}{dt}(t) = \mathbf{L}(t) \cdot \mathbf{F}(t). \tag{4}$$

Bearing in mind that

$$\frac{d\mathbf{F}^{-1}}{dt}(t) = -\mathbf{F}^{-1}(t) \cdot \frac{d\mathbf{F}}{dt}(t) \cdot \mathbf{F}^{-1}(t),$$

we find from Eq. (4) that

$$\frac{d\mathbf{F}^{-1}}{dt}(t) = -\mathbf{F}^{-1}(t) \cdot \mathbf{L}(t). \tag{5}$$

By analogy with Eqs. (4) and (5), we write

$$\frac{d\mathbf{F}_s}{dt}(t) = \mathbf{L}_s(t) \cdot \mathbf{F}_s(t), \qquad \frac{d\mathbf{F}_s^{-1}}{dt}(t) = -\mathbf{F}_s^{-1}(t) \cdot \mathbf{L}_s(t), \tag{6}$$

where

$$\mathbf{L}_s(t) = \frac{\partial \mathbf{v}_s(t)}{\partial \mathbf{r}_s(t)}$$

is the velocity gradient for sliding of junctions, and $\mathbf{v}_s(t) = d\mathbf{r}_s(t)/dt$.

It follows from Eq. (3) that

$$\frac{d\mathbf{F}_e}{dt}(t) = \frac{d}{dt}\Big[\mathbf{F}(t) \cdot \mathbf{F}_s^{-1}(t)\Big] = \frac{d\mathbf{F}}{dt}(t) \cdot \mathbf{F}_s^{-1}(t) + \mathbf{F}(t) \cdot \frac{d\mathbf{F}_s^{-1}}{dt}(t).$$

Substitution of Eqs. (4) and (6) into this equality results in

$$\frac{d\mathbf{F}_e}{dt}(t) = \mathbf{L}(t) \cdot \mathbf{F}_e(t) - \mathbf{F}_e(t) \cdot \mathbf{L}_s(t). \tag{7}$$

The left and right Cauchy–Green tensors for elastic deformation are given by

$$\mathbf{B}_e(t) = \mathbf{F}_e(t) \cdot \mathbf{F}_e^\top(t), \qquad \mathbf{C}_e(t) = \mathbf{F}_e^\top(t) \cdot \mathbf{F}_e(t), \tag{8}$$

where $\top$ stands for transpose. We differentiate the second equality in Eq. (8) with respect to time, use Eq. (7), and find that

$$\frac{d\mathbf{C}_\mathrm{e}}{dt}(t) = 2\mathbf{F}_\mathrm{e}^\top(t) \cdot \mathbf{D}(t) \cdot \mathbf{F}_\mathrm{e}(t) - \mathbf{L}_\mathrm{s}^\top(t) \cdot \mathbf{C}_\mathrm{e}(t) - \mathbf{C}_\mathrm{e}(t) \cdot \mathbf{L}_\mathrm{s}(t), \qquad (9)$$

where

$$\mathbf{D}(t) = \frac{1}{2}\Big[\mathbf{L}(t) + \mathbf{L}^\top(t)\Big] \qquad (10)$$

is the rate-of-strain tensor. Taking into account that

$$\frac{d\mathbf{C}_\mathrm{e}^{-1}}{dt}(t) = -\mathbf{C}_\mathrm{e}^{-1}(t) \cdot \frac{d\mathbf{C}_\mathrm{e}}{dt}(t) \cdot \mathbf{C}_\mathrm{e}^{-1}(t),$$

and using Eq. (9), we arrive at the formula

$$\frac{d\mathbf{C}_\mathrm{e}^{-1}}{dt}(t) = -2\mathbf{F}_\mathrm{e}^{-1}(t) \cdot \mathbf{D}(t) \cdot \Big[\mathbf{F}_\mathrm{e}^{-1}(t)\Big]^\top + \mathbf{C}_\mathrm{e}^{-1}(t) \cdot \mathbf{L}_\mathrm{s}^\top(t) + \mathbf{L}_\mathrm{s}(t) \cdot \mathbf{C}_\mathrm{e}^{-1}(t). \qquad (11)$$

The first principal invariant of the right Cauchy–Green tensor, $\mathbf{C}_\mathrm{e}(t)$, reads

$$J_1(t) = \mathbf{C}_\mathrm{e}(t) : \mathbf{I},$$

where $\mathbf{I}$ is the unit tensor and the colon stands for convolution. Differentiating this equality with respect to time and employing Eqs. (8) and (9), we obtain

$$\frac{dJ_1}{dt}(t) = 2\Big[\mathbf{B}_\mathrm{e}(t) : \mathbf{D}(t) - \mathbf{C}_\mathrm{e}(t) : \mathbf{D}_\mathrm{s}(t)\Big], \qquad (12)$$

where

$$\mathbf{D}_\mathrm{s}(t) = \frac{1}{2}\Big[\mathbf{L}_\mathrm{s}(t) + \mathbf{L}_\mathrm{s}^\top(t)\Big] \qquad (13)$$

is the rate-of-strain tensor for sliding of junctions. For an incompressible medium, the second principal invariant of the right Cauchy–Green tensor, $\mathbf{C}_\mathrm{e}(t)$, is given by

$$J_2(t) = \mathbf{C}_\mathrm{e}^{-1}(t) : \mathbf{I}.$$

Differentiation of this equality with respect to time and use of Eqs. (8) and (11) imply that

$$\frac{dJ_2}{dt}(t) = -2\Big[\mathbf{B}_\mathrm{e}^{-1}(t) : \mathbf{D}(t) - \mathbf{C}_\mathrm{e}^{-1}(t) : \mathbf{D}_\mathrm{s}(t)\Big]. \qquad (14)$$

It follows from Eqs. (12) and (14) that the derivative of an arbitrary smooth function, $\Phi(J_1, J_2)$, of the first two principal invariants of the right Cauchy–Green tensor, $\mathbf{C}_\mathrm{e}(t)$, is determined by the formula

$$\begin{aligned}
\frac{d\Phi}{dt}\big(J_1(t), J_2(t)\big) &= 2\Big\{\Big[\Phi_1(t)\mathbf{B}_\mathrm{e}(t) - \Phi_2(t)\mathbf{B}_\mathrm{e}^{-1}(t)\Big] : \mathbf{D}(t) \\
&\quad - \Big[\Phi_1(t)\mathbf{C}_\mathrm{e}(t) - \Phi_2(t)\mathbf{C}_\mathrm{e}^{-1}(t)\Big] : \mathbf{D}_\mathrm{s}(t)\Big\},
\end{aligned} \qquad (15)$$

8

where

$$\Phi_m(t) = \frac{\partial \Phi}{\partial J_m}\Big(J_1(t), J_2(t)\Big) \qquad (m = 1, 2). \tag{16}$$

To describe strain-hardening of a semicrystalline polymer under active loading in the post-yield region of deformations, we introduce the deformation gradient

$$\mathbf{f}(t) = \mathbf{F}_\mathrm{s}(t) \cdot \mathbf{F}_\mathrm{s}^{-1}(t_\mathrm{y}) \tag{17}$$

from the reference state at the yielding point to the reference state at time $t \geq t_\mathrm{y}$, where t_y is the instant when yielding occurs. It follows from Eqs. (6) and (17) that the tensor $\mathbf{f}$ obeys the linear differential equation

$$\frac{d\mathbf{f}}{dt}(t) = \mathbf{L}_\mathrm{s}(t) \cdot \mathbf{f}(t), \qquad \mathbf{f}(t_\mathrm{y}) = \mathbf{I}. \tag{18}$$

By analogy with Eq. (8), we introduce the left and right Cauchy–Green tensors for the post-yield transformation of the reference state

$$\mathbf{b}(t) = \mathbf{f}(t) \cdot \mathbf{f}^\top(t), \qquad \mathbf{c}(t) = \mathbf{f}^\top(t) \cdot \mathbf{f}(t). \tag{19}$$

Differentiating the second equality in Eq. (19) and using Eqs. (17) and (18), we obtain

$$\frac{d\mathbf{c}}{dt}(t) = 2\mathbf{f}^\top(t) \cdot \mathbf{D}_\mathrm{s}(t) \cdot \mathbf{f}(t). \tag{20}$$

Taking into account that

$$\frac{d\mathbf{c}^{-1}}{dt}(t) = -\mathbf{c}^{-1}(t) \cdot \frac{d\mathbf{c}}{dt}(t) \cdot \mathbf{c}^{-1}(t),$$

we find from Eq. (20) that

$$\frac{d\mathbf{c}^{-1}}{dt}(t) = -2\mathbf{f}^{-1}(t) \cdot \mathbf{D}_\mathrm{s}(t) \cdot \Big[\mathbf{f}^{-1}(t)\Big]^\top. \tag{21}$$

As any transformation of the reference state is volume preserving, the first two principal invariants of the tensor $\mathbf{c}(t)$ are given by

$$j_1(t) = \mathbf{c}(t) : \mathbf{I}, \qquad j_2(t) = \mathbf{c}^{-1}(t) : \mathbf{I}. \tag{22}$$

Differentiating Eqs. (22) with respect to time and using Eqs. (19) to (21), we arrive at the formulas

$$\frac{dj_1}{dt}(t) = 2\mathbf{b}(t) : \mathbf{D}_\mathrm{s}(t), \qquad \frac{dj_2}{dt}(t) = -2\mathbf{b}^{-1}(t) : \mathbf{D}_\mathrm{s}(t). \tag{23}$$

It follows from Eq. (23) that the derivative of an arbitrary smooth function, $\phi(j_1, j_2)$, of the principal invariants of the right Cauchy–Green tensor, $\mathbf{c}(t)$, reads

$$\frac{d\phi}{dt}\Big(j_1(t), j_2(t)\Big) = 2\Big[\phi_1(t)\mathbf{b}(t) - \phi_2(t)\mathbf{b}^{-1}(t)\Big] : \mathbf{D}_\mathrm{s}(t), \tag{24}$$

where

$$\phi_m(t) = \frac{\partial \phi}{\partial j_m}\Big(j_1(t), j_2(t)\Big) \qquad (m = 1, 2). \tag{25}$$

Equations (19), (22) and (24) are valid for any $t \geq t_{\mathrm{y}}$. In the sub-yield region of deformations, when $t < t_{\mathrm{y}}$, we set formally

$$\mathbf{b}(t) = \mathbf{c}(t) = \mathbf{I}, \quad j_1(t) = j_2(t) = 3, \quad \frac{d\phi}{dt}\Big(j_1(t), j_2(t)\Big) = 0. \tag{26}$$

Our aim now is to express the rate-of-strain tensor for sliding of junctions, $\mathbf{D}_{\mathrm{s}}(t)$, in terms of the rate-of-strain tensor for macro-deformation, $\mathbf{D}(t)$, and some tensors that characterize elastic deformation of a specimen.

4   Kinetics of fine slip

A semicrystalline polymer is treated as a strongly heterogeneous network of chains linked by junctions. Unlike [17], where the spatial inhomogeneity of the network is associated with micronecking driven by fragmentation of lamellar blocks, we attribute the heterogeneity of the network to an inhomogeneity of interactions between chains in the amorphous phase and crystalline lamellae with various lengths and thicknesses.

The network is thought of as an ensemble of meso-regions with arbitrary shapes and sizes. The characteristic length of a MR substantially exceeds the radius of gyration for a macromolecule, and it is noticeably less than the characteristic size of a sample.

Deformation of a specimen induces two sliding processes in the network:

1. Sliding of junctions between chains with respect to their reference positions in stress-free meso-domains.

2. Sliding of MRs in the ensemble with respect to each other.

Sliding of nodes in meso-domains of an equivalent network reflects

- sliding of junctions between chains in the amorphous phase,

- slippage of tie chains along lamellar surfaces [19],

- fine slip of crystalline lamellae (homogeneous shearing of layer-like crystallites and small displacements of lamellar blocks with respect to one another) [4].

Sliding of MRs with respect to each other describes

- coarse slip of lamellae (inter-lamellar sliding),

- fragmentation of lamellae into mosaic blocks linked by tie chains,

- their alignment along the direction of maximal stresses [4].

To describe evolution of the microstructure of a semicrystalline polymer driven by simultaneous effects of these two sliding processes, we introduce two rate-of-strain tensors, $\mathbf{D}_f$ and $\mathbf{D}_c$, and adopt the conventional assumption that the total rate-of-strain tensor, $\mathbf{D}_s$, equals the sum of $\mathbf{D}_f$ and $\mathbf{D}_c$,

$$\mathbf{D}_s = \mathbf{D}_f + \mathbf{D}_c, \tag{27}$$

where the subscript indices "f" and "c" refer to fine and coarse slip, respectively.

We suppose that deformation of a specimen induces sliding of junctions in amorphous regions and fine slip of lamellar blocks both in the sub-yield and post-yield regions of deformation. Te rate-of-strain tensor, $\mathbf{D}_f$, is assumed to be proportional to the rate-of-strain tensor, $\mathbf{D}$,

$$\mathbf{D}_f(t) = \alpha(t)\mathbf{D}(t). \tag{28}$$

For an incompressible isotropic medium, the coefficient of proportionality, α, depends on the principal invariants, J_1 and J_2, of the right Cauchy–Green tensor $\mathbf{C}_e$. This coefficient vanishes at the zero elastic strain, monotonically increases with elastic deformation, and tends to some constant $a \in [0,1]$ (the rate of sliding of junctions for a developed viscoplastic flow) at relatively large elastic strains. The inequality $a \geq 0$ means that junctions move in the direction determined by the macro-strain, whereas the condition $a \leq 1$ ensures that the rate of the steady flow of nodes does not exceed the rate of macro-strain.

Assuming the tensor $\mathbf{D}_c(t)$ to vanish in the sub-yield region of deformations and substituting Eqs. (27) and (28) into Eqs. (15) and (26), we find that for any $t < t_y$,

$$
\begin{aligned}
\frac{d\Phi}{dt}\Big(J_1(t), J_2(t)\Big) &= 2\Big[\Phi_1(t)\Big(\mathbf{B}_e(t) - \alpha(t)\mathbf{C}_e(t)\Big) \\
&\quad -\Phi_2(t)\Big(\mathbf{B}_e^{-1}(t) - \alpha(t)\mathbf{C}_e^{-1}(t)\Big)\Big] : \mathbf{D}(t), \\
\frac{d\phi}{dt}\Big(j_1(t), j_2(t)\Big) &= 0.
\end{aligned}
\tag{29}
$$

It follows from Eqs. (15), (24), (27) and (28) that in the post-yield region of deformations, when $t \geq t_y$, the derivatives of the functions Φ and ϕ read

$$
\begin{aligned}
\frac{d\Phi}{dt}\Big(J_1(t), J_2(t)\Big) &= 2\Big\{\Big[\Phi_1(t)\Big(\mathbf{B}_e(t) - \alpha(t)\mathbf{C}_e(t)\Big) \\
&\quad -\Phi_2(t)\Big(\mathbf{B}_e^{-1}(t) - \alpha(t)\mathbf{C}_e^{-1}(t)\Big)\Big] : \mathbf{D}(t) \\
&\quad -\Big[\Phi_1(t)\mathbf{C}_e(t) - \Phi_2(t)\mathbf{C}_e^{-1}(t)\Big] : \mathbf{D}_c(t)\Big\}, \\
\frac{d\phi}{dt}\Big(j_1(t), j_2(t)\Big) &= 2\alpha(t)\Big[\phi_1(t)\mathbf{b}(t) - \phi_2(t)\mathbf{b}^{-1}(t)\Big] : \mathbf{D}(t) \\
&\quad +2\Big[\phi_1(t)\mathbf{b}(t) - \phi_2(t)\mathbf{b}^{-1}(t)\Big] : \mathbf{D}_c(t),
\end{aligned}
\tag{30}
$$

where the functions Φ_m and ϕ_m ($m = 1, 2$) are given by Eqs. (16) and (25).

5   Strain energy density

We assume that the macro-strain is transmitted to individual meso-regions by links (crystalline lamellae) that connect MRs in an ensemble. A meso-region is treated as an incom-

pressible isotropic medium with the strain energy density (per unit volume)

$$\tilde{w} = \mu w,$$

where μ is an average rigidity of a meso-domain and $w = w(J_1, J_2)$ is a dimensionless function that satisfies the condition

$$w(J_1, J_2)\Big|_{J_1=3, J_2=3} = 0.$$

This equality means that the mechanical energy of a MR vanishes in the reference state.

It is postulated that the rigidity, μ, is constant in the sub-yield region, and it monotonically increases with viscoplastic strains in the post-yield region of deformations, where μ becomes a function of the principal invariants of the right Cauchy–Green tensor $\mathbf{c}$: $\mu = \mu(j_1, j_2)$. This dependence reflects strain-hardening of a semicrystalline polymer induced by texture formation.

We adopt the conventional assumptions that (i) the excluded-volume effect and other multi-chain effects are screened for an individual chain in a network by surrounding macromolecules, and (ii) the energy of interaction between chains in a meso-region and between meso-domains can be taken into account with the help of the incompressibility condition. These hypotheses imply that the strain energy density (per unit volume) of a network, W, equals the sum of the mechanical energies of MRs,

$$W(t) = M\Big(j_1(t), j_2(t)\Big) w\Big(J_1(t), J_2(t)\Big), \tag{31}$$

where $M = \mu N$ is the rigidity of the network, and N is the average number of MRs per unit volume.

Differentiating Eq. (31) with respect to time, using Eq. (29), and taking into account that the first principal invariant of the rate-of-strain tensor, $\mathbf{D}$, valishes for isochoric deformations, we find that in the sub-yield region of deformations, when $t < t_{\mathrm{y}}$,

$$\frac{dW}{dt}(t) = \mathbf{A}'(t) : \mathbf{D}(t), \tag{32}$$

where the prime stands for the deviatoric component of a tensor,

$$\mathbf{A}(t) = 2M_0(0)\Big[w_1(t)\Big(\mathbf{B}_{\mathrm{e}}(t) - \alpha(t)\mathbf{C}_{\mathrm{e}}(t)\Big) - w_2(t)\Big(\mathbf{B}_{\mathrm{e}}^{-1}(t) - \alpha(t)\mathbf{C}_{\mathrm{e}}^{-1}(t)\Big)\Big]. \tag{33}$$

Bearing in mind that the first principal invariants of the rate-of-strain tensors, $\mathbf{D}$ and $\mathbf{D}_{\mathrm{c}}$, equal zero for a volume-preserving transformation, we find from Eqs. (30) and (31) that in the post-yield region of deformations, when $t \geq t_{\mathrm{y}}$,

$$\frac{dW}{dt}(t) = \mathbf{A}'(t) : \mathbf{D}(t) - \mathbf{A}'_{\mathrm{c}}(t) : \mathbf{D}_{\mathrm{c}}(t), \tag{34}$$

where

$$\begin{aligned}
\mathbf{A}(t) &= 2\Big\{M_0(t)\Big[w_1(t)\Big(\mathbf{B}_{\mathrm{e}}(t) - \alpha(t)\mathbf{C}_{\mathrm{e}}(t)\Big) - w_2(t)\Big(\mathbf{B}_{\mathrm{e}}^{-1}(t) - \alpha(t)\mathbf{C}_{\mathrm{e}}^{-1}(t)\Big)\Big] \\
&\quad + \alpha(t)w_0(t)\Big[M_1(t)\mathbf{b}(t) - M_2(t)\mathbf{b}^{-1}(t)\Big]\Big\}, \\
\mathbf{A}_{\mathrm{c}}(t) &= 2\Big\{M_0(t)\Big[w_1(t)\mathbf{C}_{\mathrm{e}}(t) - w_2(t)\mathbf{C}_{\mathrm{e}}^{-1}(t)\Big] - w_0(t)\Big[M_1(t)\mathbf{b}(t) - M_2(t)\mathbf{b}^{-1}(t)\Big]\Big\}. \tag{35}
\end{aligned}$$

12

The functions $w_m(t)$ and $M_m(t)$ ($m = 0, 1, 2$) in Eqs. (33) and (35) read

$$w_0(t) = w\Big(J_1(t), J_2(t)\Big), \qquad w_m(t) = \frac{\partial w}{\partial J_m}\Big(J_1(t), J_2(t)\Big),$$

$$M_0(t) = M\Big(j_1(t), j_2(t)\Big), \qquad M_m(t) = \frac{\partial M}{\partial j_m}\Big(j_1(t), j_2(t)\Big). \tag{36}$$

Our purpose now is to derive stress–strain relations for a semicrystalline polymer and kinetic equations for the evolution of the rate-of-strain tensor, $\mathbf{D}_c(t)$, in the post-yield region of deformations by using the laws of thermodynamics.

6 Constitutive equations

For isothermal deformation of an incompressible medium at a reference temperature T_0, the Clausius-Duhem inequality reads [40]

$$T_0 \frac{dQ}{dt}(t) = -\frac{dW}{dt}(t) + \mathbf{\Sigma}'(t) : \mathbf{D}(t) \geq 0, \tag{37}$$

where $\mathbf{\Sigma}$ is the Cauchy stress tensor, and Q is the entropy production per unit volume.

Substition of Eqs. (32) and (34) into Eq. (37) implies that in the sub-yield region of deformations, when $t < t_y$,

$$T_0 \frac{dQ}{dt}(t) = \Big[\mathbf{\Sigma}(t) - \mathbf{A}(t)\Big]' : \mathbf{D}(t), \tag{38}$$

whereas in the post-yield region, when $t \geq t_y$,

$$T_0 \frac{dQ}{dt}(t) = \Big[\mathbf{\Sigma}(t) - \mathbf{A}(t)\Big]' : \mathbf{D}(t) + \mathbf{A}'_c(t) : \mathbf{D}_c(t). \tag{39}$$

The main hypothesis of the present study is that

- sliding of nodes in the amorphous phase and fine slip of lamellar blocks do not induce dissipation of mechanical energy,

- an increase in the specific entropy of an equivalent network is driven by coarse slip and fragmentation of lamellae only.

This assumption implies that in the sub-yield region of deformations,

$$\frac{dQ}{dt}(t) = 0. \tag{40}$$

The entropy production in the post-yield region of deformations is attributed to the coarse slip of lamellar blocks characterized by the rate-of-strain tensor $\mathbf{D}_c$. Adopting the conventional formula for the rate of entropy production driven by a viscoplastic flow, we find that

$$\frac{dQ}{dt}(t) = \frac{1}{\gamma T_0 D_i(t)} \mathbf{D}_c(t) : \mathbf{D}_c(t), \tag{41}$$

13

where γ is the rate of viscoplastic flow and

$$D_{\mathrm{i}} = \left(\frac{2}{3}\mathbf{D} : \mathbf{D}\right)^{\frac{1}{2}} \tag{42}$$

is the intensity of macro-strain rate.

Substitution of expression (40) into Eq. (38) implies that for an arbitrary loading program, the Clausius–Duhem inequality is satisfied in the sub-yield region of deformations, provided that the Cauchy stress tensor, $\mathbf{\Sigma}$, reads

$$
\begin{aligned}
\mathbf{\Sigma}(t) &= -p(t)\mathbf{I} + 2M_0(0)\Big[w_1(t)\big(\mathbf{B}_{\mathrm{e}}(t) - \alpha(t)\mathbf{C}_{\mathrm{e}}(t)\big) \\
&\quad -w_2(t)\big(\mathbf{B}_{\mathrm{e}}^{-1}(t) - \alpha(t)\mathbf{C}_{\mathrm{e}}^{-1}(t)\big)\Big],
\end{aligned}
\tag{43}
$$

where $p(t)$ is pressure.

It follows from Eqs. (39) and (41) that for an arbitrary loading program, the Clausius–Duhem inequality is satisfied in the post-yield region of deformations provided that the Cauchy stress tensor, $\mathbf{\Sigma}$, is given by

$$
\begin{aligned}
\mathbf{\Sigma}(t) &= -p(t)\mathbf{I} + 2\Big\{M_0(t)\Big[w_1(t)\big(\mathbf{B}_{\mathrm{e}}(t) - \alpha(t)\mathbf{C}_{\mathrm{e}}(t)\big) \\
&\quad -w_2(t)\big(\mathbf{B}_{\mathrm{e}}^{-1}(t) - \alpha(t)\mathbf{C}_{\mathrm{e}}^{-1}(t)\big)\Big] \\
&\quad +\alpha(t)w_0(t)\Big[M_1(t)\mathbf{b}(t) - M_2(t)\mathbf{b}^{-1}(t)\Big]\Big\}
\end{aligned}
\tag{44}
$$

and the rate-of-strain tensor for coarse slip of lamellar blocks is determined by the formula

$$
\begin{aligned}
\mathbf{D}_{\mathrm{c}}(t) &= 2\gamma\Big\{M_0(t)\Big[w_1(t)\mathbf{C}_{\mathrm{e}}(t) - w_2(t)\mathbf{C}_{\mathrm{e}}^{-1}(t)\Big] \\
&\quad -w_0(t)\Big[M_1(t)\mathbf{b}(t) - M_2(t)\mathbf{b}^{-1}(t)\Big]\Big\}' D_{\mathrm{i}}(t).
\end{aligned}
\tag{45}
$$

Equation (45) implies that the rate-of-strain tensor for viscoplastic flow in the post-yield region, $\mathbf{D}_{\mathrm{c}}$, is proportional to the intensity of the rate-of-strain tensor for macro-deformation, $\mathbf{D}$.

The set of constitutive equations for a semicrystalline polymer consists of the stress–strain relations (43) and (44) together with the kinetic equations (27), (28) and (45) for fine and coarse slip of lamellar blocks. The governing equations are determined by 3 material functions: $\alpha(t)$, $M(j_1, j_2)$ and $w(J_1, J_2)$.

For an arbitrary three-dimensional deformation, the set of governing equations should be completed by a relationship between the vorticity tensor for the viscoplastic flow, $\mathbf{\Omega}_s(t) = \frac{1}{2}[\mathbf{L}_s^\top - \mathbf{L}_s(t)]$, and the vorticity tensor for macro-deformation, $\mathbf{\Omega}(t) = \frac{1}{2}[\mathbf{L}^\top - \mathbf{L}(t)]$. We do not dwell, however, on such a relation, because this work focuses on uniaxial tension of an incompressible medium, when the tensors, $\mathbf{\Omega}$ and $\mathbf{\Omega}_s$, vanish.

7   Material functions

The dimensionless strain energy density, w, is given by

$$w = J_1 - 3. \tag{46}$$

14

Equation (46) describes the mechanical energy of a neo-Hookean medium. The advantages of this equation are that it (i) contains no adjustable parameters, and (ii) has a transparent physical meaning as the strain energy density of a Gaussian network of flexible chains [41].

The following phenomenological relation is proposed for the function $\alpha(t)$:

$$\alpha = a\Big[1 - \exp\Big(-\frac{\sqrt{J_1 - 3}}{\varepsilon}\Big)\Big]. \tag{47}$$

Formula (47) is determined by two adjustable parameters, a and ε: the coefficient a is the rate of sliding of junctions for a developed viscoplastic flow, and the strain ε characterizes transition to the steady flow. Equation (47) was successfully employed in our previous study on the viscoplastic response of iPP at small strains [42]. Similar relation was suggested in [43] to describe the time-dependent response of polyethylene melts.

To describe changes in the elastic modulus, M, induced by texture formation in the post-yield region of deformations, we adopt the phenomenological equation

$$M(j_1, j_2) = \frac{1}{2}E\Big[1 + \eta(j_1 - 3)\Big]. \tag{48}$$

An advantage of Eq. (48) is that it is determined by two adjustable parameters, E and η, and the effect of viscoplastic flow on the elastic modulus is accounted in a fashion similar to that employed in Eqs. (46) and (47).

As this work focuses on experimental data in uniaxial tensile tests, an explicit expression for the yield surface cannot be verified. We accept the von Mises criterion and assume that in the sub-yield region of deformations,

$$\Sigma_i < \Sigma_y,$$

whereas in the post-yield region,

$$\Sigma_i \geq \Sigma_y,$$

where

$$\Sigma_i = \Big(\frac{3}{2}\mathbf{\Sigma}' : \mathbf{\Sigma}'\Big)^{\frac{1}{2}} \tag{49}$$

is the true stress intensity.

Substituting expressions (46) and (48) into Eqs. (43) to (45) and using Eq. (36), we find that in the sub-yield region of deformations,

$$
\begin{aligned}
\mathbf{\Sigma}(t) &= -p(t)\mathbf{I} + E\Big[\mathbf{B}_e(t) - \alpha(t)\mathbf{C}_e(t)\Big], \\
\mathbf{D}_s(t) &= \alpha(t)\mathbf{D}(t),
\end{aligned} \tag{50}
$$

and in the post-yield region of deformations,

$$
\begin{aligned}
\mathbf{\Sigma}(t) &= -p(t)\mathbf{I} + E\Big\{\Big[1 + \eta\big(j_1(t) - 3\big)\Big]\Big[\mathbf{B}_e(t) - \alpha(t)\mathbf{C}_e(t)\Big] \\
&\quad + \eta\alpha(t)\big(J_1(t) - 3\big)\mathbf{b}(t)\Big\}, \\
\mathbf{D}_s(t) &= \alpha(t)\mathbf{D}(t) + \gamma E D_i(t)\Big\{\Big[1 + \eta\big(j_1(t) - 3\big)\Big]\mathbf{C}_e(t) \\
&\quad - \eta\big(J_1(t) - 3\big)\mathbf{b}(t)\Big\}'.
\end{aligned} \tag{51}
$$

The stress–strain relations (50) and (51) are determined by 5 adjustable parameters: a, E, γ, η and ε. An advantage of this model is that the number of constants to be found by fitting experimental data is substantially smaller than that in other constitutive relations in finite viscoplasticity of solid polymers [23, 25, 30, 44, 45, 46, 47, 48].

Our purpose now is to simplify the stress–strain relations for uniaxial tension of an incompressible medium.

8 Uniaxial tension

Points of a bar refer to Cartesian coordinates $\{X_i\}$ ($i = 1, 2, 3$) in the stress-free state, to Cartesian coordinates $\{x_i\}$ in the deformed state, and to Cartesian coordinates $\{\xi_i\}$ in the reference state at time t. Uniaxial tension of the incompressible medium is described by the formulas

$$x_1 = k(t)X_1, \qquad x_2 = k^{-\frac{1}{2}}(t)X_2, \qquad x_3 = k^{-\frac{1}{2}}(t)X_3, \tag{52}$$

where $k = k(t)$ is an elongation ratio. It is assumed that transformation of the reference state is determined by the equations similar to Eq. (52),

$$\xi_1 = \kappa(t)X_1, \qquad \xi_2 = \kappa^{-\frac{1}{2}}(t)X_2, \qquad \xi_3 = \kappa^{-\frac{1}{2}}(t)X_3, \tag{53}$$

where $\kappa(t)$ is a function to be found. It follows from Eqs. (2), (3), (8), (52) and (53) that

$$\mathbf{B}_{\mathrm{e}} = \mathbf{C}_{\mathrm{e}} = \left(\frac{k}{\kappa}\right)^2 \mathbf{e}_1\mathbf{e}_1 + \frac{\kappa}{k}(\mathbf{e}_2\mathbf{e}_2 + \mathbf{e}_3\mathbf{e}_3), \tag{54}$$

where $\mathbf{e}_i$ are base vectors of the Cartesian frame $\{X_i\}$. By analogy with Eq. (54), we find that in the post-yield region of deformations,

$$\mathbf{b} = \mathbf{c} = \left(\frac{\kappa}{\kappa_{\mathrm{y}}}\right)^2 \mathbf{e}_1\mathbf{e}_1 + \frac{\kappa_{\mathrm{y}}}{\kappa}\left(\mathbf{e}_2\mathbf{e}_2 + \mathbf{e}_3\mathbf{e}_3\right), \tag{55}$$

where κ_{y} is the value of κ at the yield point. It follows from Eqs. (22), (54) and (55) that

$$J_1(k, \kappa) = \left(\frac{k}{\kappa}\right)^2 + 2\frac{\kappa}{k}, \qquad j_1(\kappa, \kappa_{\mathrm{y}}) = \left(\frac{\kappa}{\kappa_{\mathrm{y}}}\right)^2 + 2\frac{\kappa_{\mathrm{y}}}{\kappa}. \tag{56}$$

Substitution of Eqs. (54) and (55) into Eqs. (50) and (51) implies that

$$\boldsymbol{\Sigma} = \Sigma_1\mathbf{e}_1\mathbf{e}_1 + \Sigma_2(\mathbf{e}_2\mathbf{e}_2 + \mathbf{e}_3\mathbf{e}_3).$$

In the sub-yield region of deformations, the non-zero components of the Cauchy stress tensor, Σ_1 and Σ_2, are given by

$$\begin{aligned}
\Sigma_1 &= -p(k, \kappa) + E\Big[1 - \alpha(k, \kappa)\Big]\left(\frac{k}{\kappa}\right)^2, \\
\Sigma_2 &= -p(k, \kappa) + E\Big[1 - \alpha(k, \kappa)\Big]\frac{\kappa}{k}.
\end{aligned} \tag{57}$$

In the post-yield region of deformations, these quantities read

$$
\begin{aligned}
\Sigma_1 &= -p(k, \kappa, \kappa_{\mathrm{y}}) + E\Big\{\big[1 - \alpha(k, \kappa)\big]\big[1 + \eta\big(j_1(\kappa, \kappa_{\mathrm{y}}) - 3\big)\big]\Big(\frac{k}{\kappa}\Big)^2 \\
&\quad + \eta\alpha(k, \kappa)\big(J_1(k, \kappa) - 3\big)\Big(\frac{\kappa}{\kappa_{\mathrm{y}}}\Big)^2\Big\},
\end{aligned}
$$

$$
\begin{aligned}
\Sigma_2 &= -p(k, \kappa, \kappa_{\mathrm{y}}) + E\Big\{\big[1 - \alpha(k, \kappa)\big]\big[1 + \eta\big(j_1(\kappa, \kappa_{\mathrm{y}}) - 3\big)\big]\frac{\kappa}{k} \\
&\quad + \eta\alpha(k, \kappa)\big(J_1(k, \kappa) - 3\big)\frac{\kappa_{\mathrm{y}}}{\kappa}\Big\},
\end{aligned} \tag{58}
$$

where the function $\alpha(k, \kappa)$ is given by Eqs. (47) and (56).

Excluding the unknown pressure, p, from Eqs. (57) and (58) and the boundary condition, $\Sigma_2 = 0$, on the lateral surface of the bar, we find the only component of the Cauchy stress tensor, the true longitudinal stress $\Sigma = \Sigma_1$. Bearing in mind that for uniaxial tension of an incompressible medium, $\Sigma_{\mathrm{i}} = \Sigma$, we obtain

$$
\begin{aligned}
\Sigma &= E\big[1 - \alpha(k, \kappa)\big]\Big[\Big(\frac{k}{\kappa}\Big)^2 - \frac{\kappa}{k}\Big] \qquad (\Sigma < \Sigma_{\mathrm{y}}), \\
\Sigma &= E\Big\{\big[1 - \alpha(k, \kappa)\big]\big[1 + \eta\big(j_1(\kappa, \kappa_{\mathrm{y}}) - 3\big)\big]\Big[\Big(\frac{k}{\kappa}\Big)^2 - \frac{\kappa}{k}\Big] \\
&\quad + \eta\alpha(k, \kappa)\big(J_1(k, \kappa) - 3\big)\Big[\Big(\frac{\kappa}{\kappa_{\mathrm{y}}}\Big)^2 - \frac{\kappa_{\mathrm{y}}}{\kappa}\Big]\Big\} \qquad (\Sigma \geq \Sigma_{\mathrm{y}}).
\end{aligned} \tag{59}
$$

Equations (10), (13), (52) and (53) result in the formulas

$$
\mathbf{D} = \frac{1}{k}\frac{dk}{dt}\Big[\mathbf{e}_1\mathbf{e}_1 - \frac{1}{2}(\mathbf{e}_2\mathbf{e}_2 + \mathbf{e}_3\mathbf{e}_3)\Big], \qquad \mathbf{D}_{\mathrm{s}} = \frac{1}{\kappa}\frac{d\kappa}{dt}\Big[\mathbf{e}_1\mathbf{e}_1 - \frac{1}{2}(\mathbf{e}_2\mathbf{e}_2 + \mathbf{e}_3\mathbf{e}_3)\Big], \tag{60}
$$

which, together with Eq. (42), imply that

$$
D_{\mathrm{i}} = \frac{1}{k}\frac{dk}{dt}. \tag{61}
$$

It follows from Eqs. (50), (51), (60) and (61) that

$$
\begin{aligned}
\frac{d\kappa}{dk} &= \alpha(k, \kappa)\frac{\kappa}{k} \qquad (\Sigma < \Sigma_{\mathrm{y}}), \\
\frac{d\kappa}{dk} &= \frac{\kappa}{k}\Big\{\alpha(k, \kappa) + \Gamma\Big[\big(1 + \eta\big(j_1(\kappa, \kappa_{\mathrm{y}}) - 3\big)\big)\Big(\Big(\frac{k}{\kappa}\Big)^2 - \frac{\kappa}{k}\Big) \\
&\quad - \eta\big(J_1(k, \kappa) - 3\big)\Big(\Big(\frac{\kappa}{\kappa_{\mathrm{y}}}\Big)^2 - \frac{\kappa_{\mathrm{y}}}{\kappa}\Big)\Big]\Big\} \qquad (\Sigma \geq \Sigma_{\mathrm{y}})
\end{aligned} \tag{62}
$$

with $\Gamma = \frac{2}{3}\gamma E$.

Given a loading program, $k = k(t)$, the longitudinal stress, $\Sigma(t)$, is determined by Eq. (59). The elongation ratio, $\kappa(t)$, that characterizes fine and coarse slips of lamellar blocks, is found from the nonlinear differential equations (62) with the initial condition $\kappa(1) = 1$. The constitutive equations involve 5 adjustable parameters:

1. the elastic modulus E,

2. the rate of a developed viscoplastic flow of junctions a,

3. the strain ε that characterizes transition to a steady flow of junctions,

4. the rate of coarse slip of lamellar blocks Γ,

5. the coefficient η that characterizes strain-hardenig in the post-yield region of deformations.

The yield stress, Σ_y, is determined directly from a stress–strain diagram as the true stress corresponding to the point of maximum on the engineering stress–engineering strain curve. To find the viscoplastic elongation ratio at yielding, κ_y, the constitutive equations are integrated from $\Sigma = 0$ to $\Sigma = \Sigma_y$.

An important advantage of Eqs. (59) and (62) is that 3 material constants, E, a and ε, are found by fitting a stress–strain curve below the yield point. Afterwards, the other two parameters, Γ and η, are determined by matching the stress–strain curve in the post-yield region of deformations.

9 Fitting of observations

We begin with matching the stress–strain diagrams below the apparent yield point. To find the constants E, a and ε, we fix some intervals $[0, a_{\max}]$ and $[0, \varepsilon_{\max}]$, where the "best-fit" parameters a and ε are assumed to be located, and divide these intervals into J subintervals by the points $a^{(i)} = i\Delta a$ and $\varepsilon^{(j)} = j\Delta\varepsilon$ $(i, j = 1, \ldots, J)$ with $\Delta a = a_{\max}/J$ and $\Delta\varepsilon = \varepsilon_{\max}/J$. For any pair, $\{a^{(i)}, \varepsilon^{(j)}\}$, Eqs. (59) and (62) are integrated numerically by the Runge–Kutta method with the step $\Delta k = 1.0 \cdot 10^{-5}$ in the interval between $\Sigma = 0$ and $\Sigma = \Sigma_y$. Given a pair, $\{a^{(i)}, \varepsilon^{(j)}\}$, the elastic modulus, E, is found by the least-squares method from the condition of minimum of the function

$$R = \sum_{k_n} \Big[\Sigma_{\exp}(k_n) - \Sigma_{\text{num}}(k_n)\Big]^2,$$

where the sum is calculated over all experimental points, k_n, in the sub-yield interval, $\Sigma_{\exp}$ is the stress measured in a tensile test, and Σ_{num} is given by Eq. (59). The "best-fit" parameters a and ε are determined from the condition of minimum of the function R on the set $\{a^{(i)}, \varepsilon^{(j)} \quad (i, j = 1, \ldots, J)\}$.

The material constants E, a and ε that minimize the discrepancies between the experimental data and the results of numerical analysis are found for any stress–strain curve independently.

First, we approximate the observations for non-annealed specimens. Figures 1 to 7 demonstrate good quality of fitting the stress–strain curves up to the points of necking formation. This result is rather surprising. In terms of the model, it means that for samples not subjected to thermal treatment, necking (transition from a homogeneous to a spatially heterogeneous deformation of samples) precedes yielding (coarse slip and fragmentation of

lamellar blocks). This implies that the presence of a wide plateau on a stress–strain diagram for a non-annealed specimen near the point of maximum may be attributed not to the material yielding (as conventional scenarios for yielding suggest), but to a developed flow of junctions in the amorphous phase and fine slip of lamellar blocks in the crystalline phase without lamellar fragmentation and texture formation.

Afterwards, we match the stress–strain curves in the sub-yield region of deformations for annealed specimens. Figures 8 to 14 show fair agreement between the experimental data and the results of numerical analysis.

The adjustable parameters E, a and ε are plotted versus the rate of Hencky strain, $\dot{\epsilon}_{\mathrm{H}}$, in Figures 16 to 18. The experimental data are fitted by the functions

$$E = E_0 + E_1 \log \dot{\epsilon}_{\mathrm{H}}, \qquad a = a_0 + a_1 \log \dot{\epsilon}_{\mathrm{H}}, \qquad \log \varepsilon = \varepsilon_0 + \varepsilon_1 \log \dot{\epsilon}_{\mathrm{H}}, \tag{63}$$

where the coefficients E_m, a_m and ε_m ($m = 0, 1$) are found by the least-square technique. Figures 16 to 18 demonstrate acceptable agreement between the observations and their approximations by phenomenological relations (63). It is worth noting rather large scatter of the experimental data for annnealed samples compared to that for specimens not subjected to thermal pre-treatment. These discrepancies may be explained by a substantial decrease in the interval of elongation ratios where the fitting procedure is performed (the maximal engineering strain for the interval where the stress–strain curves are approximated is reduced by a factor of three: from 0.15 to 0.05).

To find the quantities Γ and η, we approximate the stress–strain curves for annealed specimens in the post-yield region of deformation. For any set of experimental data, we use the parameters E, a and ε found by fitting an appropriate stress–strain curve in the sub-yield region of deformations. To approximate a stress–strain curve above the yield point, we apply an algorithm similar to that used to match the observations in the sub-yield region of deformations. We fix some intervals $[0, \Gamma_{\max}]$ and $[0, \eta_{\max}]$, where the "best-fit" parameters Γ and η are assumed to be located, and divide these intervals into J subintervals by the points $\Gamma^{(i)} = i\Delta\Gamma$ and $\eta^{(j)} = j\Delta\eta$ ($i, j = 1, \ldots, J$) with $\Delta\Gamma = \Gamma_{\max}/J$ and $\Delta\eta = \eta_{\max}/J$. Given a pair, $\{\Gamma^{(i)}, \eta^{(j)}\}$, Eqs. (59) and (62) are integrated numerically by the Runge–Kutta method with the step $\Delta k = 1.0 \cdot 10^{-5}$. The "best-fit" parameters Γ and η are found from the condition of minimum of the function R on the set $\{\Gamma^{(i)}, \eta^{(j)} \quad (i, j = 1, \ldots, J)\}$.

The dimensionless parameters, Γ and η, are plotted versus the Hencky strain rate, $\dot{\epsilon}_{\mathrm{H}}$, in Figures 19 and 20. The observations for the rate of coarse slip of lamellar blocks show that Γ is constant, $\Gamma = \Gamma_0$. The experimental data for the parameter η are approximated by the function

$$\eta = \eta_0 + \eta_1 \log \dot{\epsilon}_{\mathrm{H}}, \tag{64}$$

where the coefficients η_m ($m = 0, 1$) are found by the least-squares algorithm. Figure 20 demonstrates that Eq. (64) ensures acceptable quality of matching the observations.

10 Discussion

Figures 1 to 14 demonstrate fair agreement between the experimental data in uniaxial tensile tests and the results of numerical simulation, which means that the constitutive equations can be successfully applied to fit observations for isotactic polypropylene (non-annealed

as well as subjected to thermal pre-treatment) at various strain rates and elongation ratios. This conclusion contradicts the conventional standpoint [41] that (i) the concept of Gaussian networks of flexible chains (which implies Eq. (46) for the mechanical energy per unit volume) fails to correctly approximate stress–strain curves for solid polymers at finite strains and (ii) more sophisticated expressions are necessary for the strain energy density w (based on either the slip-link theory [15, 17, 25] or a multi-chain version of the theory of polymeric networks with finite extensibility of chains [7, 28, 30, 44]). Within the model proposed, an acceptable quality of matching observations is reached based on the hypotheses about (i) non-affine motion of nodes in the network and (ii) the growth of the elastic modulus driven by texture formation.

Figure 16 reveals that the elastic modulus, E, monotonically increases with the rate of stretching for non-annealed specimens and decreases for annealed samples. The following explanations may be provided for this finding.

As the present study concentrates on the viscoplastic behavior of semicrystalline polymers, we disregard the viscoelastic phenomena associated with rearrangement of chains (separation of active strands from junctions and merging of dangling strands with the network) and treat a polymer as an equivalent network of chains bridged by permanent junctions. Given a strain rate, the simplest way to account for these effects is to distinguish between two groups of meso-regions in an ensemble:

- the characteristic time for rearrangement of chains in MRs belonging to the first group is substantially smaller than the characteristic time of loading (which means that the contribution of these meso-domains into the strain energy of a polymer is negligible),

- the characteristic time for rearrangement of chains in MRs of the other group exceeds the characteristic time for loading (which implies that rearrangement of chains in these meso-domains may be disregarded and they may be considered as permanent networks).

According to this division of MRs into two groups, the number of meso-regions with permanent junctions per unit volume, N, in the formula for the elastic modulus, E, grows with the Hencky strain rate $\dot{\epsilon}_H$ (because an increase in $\dot{\epsilon}_H$ results in a decrease in the characteristic time of loading, and, as a consequence, a decrease in the content of MRs where stresses in chains relax due to the rearrangement process). This conclusion is in agrement with the experimental data presented in Figure 16 for non-annealed specimens (curve 1). When the cross-head speed decreases from 200 to 5 mm/min (which corresponds to an increase in the loading time from 4 to 180 s), the elastic modulus, E, is reduced by about 15%, which is quite comparable with the intensity of decay in the longitudinal stress during 180 s in uniaxial tensile relaxation tests [38].

The substantial decrease in the elastic modulus of annealed specimens with the Hencky strain rate (curve 2 in Figure 16) may be associated with alteration of the morphological structure of iPP at thermal treatment.

Stretching of a semicrystalline polymer in the sub-yield region of deformations activates sliding of junctions in amorphous domains between lamellae. Displacements of junctions induce separation of tie chains from crystallites and their slippage along lamellar blocks. When the tie chains are rather long, they have enough time to attach to lamellae in new cites, which

implies that the total number of links between amorphous regions and crystalline lamellae (than transmit the macro-strain to amorphous domains) remains practically constant. The latter means that amorphous meso-domains do not separate from the ensemble at stretching of a non-annealed specimen.

The situation changes dramatically when a semicrystalline polymer is subjected to thermal pre-treatment. Annealing of iPP for 51 h at 160 °C results in a noticeable increase in the degree of crystallinity. Crystallization of polymeric chains in amorphous regions occurs strongly inhomogeneously: long tie strands (that have high molecular mobility) are mainly crystallized, whereas majority of short tie chains remain in the amorphous state. This implies that the average length of a tie strand substantially decreases at thermal treatment. Sliding of junctions in amorphous domains caused by straining of a specimen induces separation of tie chains from crystallites and their slippage along lamellar surfaces. Unlike non-annealed specimens, where tie chains are rather long (which implies that their mobility is high and the time necessary for their reconnection is small), for annealed samples, the rate of attachment of short tie chains (with low molecular mobility) to new cites on the surfaces of crystallites becomes comparable with the strain rate. This means that an increase in the Hencky strain rate, $\dot{\epsilon}_H$, results in a strong decrease in the concentration of links that transmit the macro-strain to amorphous domains. As a consequence, individual MRs separate from the ensemble (due to the breakage of links between amorphous meso-domains and surrounding regions), which implies that the number of "active" meso-regions per unit volume, N, decreases with $\dot{\epsilon}_H$. As the elastic modulus, E, is proportional to N, the growth of the strain rate induces a decrease the elastic modulus of annealed specimens, in accord with the experimental data depicted in Figure 16 (curve 2).

It is worth noting that at small strain rates (when detachment of tie chains from lamellar blocks is not pronounced) the elastic modulus, E, of samples subjected to thermal treatment substantially (about by twice) exceeds that of non-annealed specimens (due to the growth in the degree of crystallinity). With an increase in the Hencky strain rate, the difference between the moduli of annealed and non-annealed samples is reduced, and at relatively high strain rates (above $\dot{\epsilon}_c \approx 5 \cdot 10^{-2}$ s^{-1}), the elastic modulus of non-annealed specimens exceeds that of annealed ones.

Figure 17 shows that the dimensionless rate of a developed flow of junctions, a, monotonically increases with the strain rate. This phenomenon may be ascribed to breakage of tie chains that bridge amorphous regions with lamellar blocks. A decrease in the concentration of these chains implies that the mobility of junctions in amorphous MRs grows, which is observed as an increase in a with $\dot{\epsilon}_H$. At small strain rates (below the threshold value, $\dot{\epsilon}_c$), the rate of a steady viscoplastic flow, a, for non-annealed specimens exceeds that for samples subjected to thermal treatment (this observation is ascribed to the secondary crystallization at annealing that reduces molecular mobility in meso-regions), whereas at high strain rates (that exceed $\dot{\epsilon}_c$), the inverse picture is revealed (the rate of a developed flow of junctions for annealed specimens reaches its ultimate value, $a = 1$). In agreement with our explanation for the decrease in the elastic modulus, E, of annealed specimens with $\dot{\epsilon}_H$, this result is attributed to breakage of tie chains (which have no time enough for their reconnection). A decrease in the content of tie chains implies a strong increase in molecular mobility in amorphous meso-regions, which is reflected by the model as the growth of the rate of viscoplastic flow a.

According to Figure 18, the strain, ε, that characterizes transition to a developed flow of junctions, increases with the rate of straining both for non-annealed and annealed specimens. It is worth noting that the increase in ε is more pronounced for annealed samples than for non-annealed ones (however, in the former case, the scatter of experimental data is rather large).

Figure 19 demonstrates that the rate, Γ, of coarse slip and fragmentation of lamellar blocks in the post-yield region of deformations is independent of the strain rate. This results appears to be quite natural: it means that the energy necessary for disintegration of lamellar blocks exceeds substentially the elastic energy stored in the semicrystalline polymer, which implies that the rate of coarse slip is not affected noticeably by mechanical factors. These factors do affect, however, the process of lamellar fragmentation, because, in accord with Eqs. (59) and (62), the derivative, $d\kappa/dk$, is proportional to the longitudinal stress, Σ.

Figure 20 reveals that the dimensionless parameter η (that characterizes strain-hardening of a semicrystalline polymer) monotonocally increases with the Hencky strain rate, $\dot{\epsilon}_{\mathrm{H}}$. This assertion appears to be quite natural. Figure 16 shows that the content of tie chains in annealed specimens decreases with the strain rate. As a consequence of this reduction in the concentration of tie chains, broken lamellar blocks become more mobile, and they are oriented easier along the direction of the longitudinal stress. The strain-rate induced intensification of the alignment process for disintegrated lamellar blocks implies a more pronounced increase in the stress, Σ, with the elongation ratio, k, in the post-yield region of deformations observed in Figure 20.

According to Eq. (48) and Figure 20, the growth of the elastic modulus, E, driven by strain-hardening of iPP (in tensile tests with the maximal Hencky strain $\epsilon_{\mathrm{H}} = 0.6$) is of order of few per cent. It is worth noting that the same (qualitatively) level of orientation of lamellar blocks was recently observed in SAXS (small angle X-ray scattering) measurements on another semicrystalline polymer (polyamide PA11) at uniaxial tension up to the necking point [49].

11 Concluding remarks

Two series of uniaxial tensile tests have been performed on isotactic polypropylene at room temperature. The first series of experiments is carried out on injection-molded specimens non-subjected to thermal treatment. In the other series of tests, the samples were annealed for 51 h at the temperature $T = 160\,^{\circ}\mathrm{C}$ prior to loading. Each series consists of 7 experiments with the cross-hear speeds ranging from 5 to 200 mm/min (which cover practically the entire range of cross-head speeds employed in conventional quasi-static tensile tests). Stretching of a non-annealed specimen is performed up to the onset of necking. Deformation of a sample subjected to thermal treatment is carried out up to the maximal Hencky strain $\epsilon_{\mathrm{H}} = 0.6$.

Constitutive equations have been derived for the isothermal viscoplastic behavior of a semicrystalline polymer at finite strains. A polymer is treated as an equivalent heterogeneous network of chains bridged by permanent junctions. The network is thought of as an ensemble of meso-regions linked with each other. Under loading, junctions between chains in MRs move with respect to their reference positions (this process reflects sliding of nodes in the amorphous phase and fine slip of lamellar blocks). At relatively large elongations, the sliding

process is accompanied by displacement of meso-regions with respect to each other (which reflects coarse slip and fragmentation of lamellar blocks).

Unlike the conventional definition of the yield point of a solid polymer at uniaxial tension as the point of maximum on the engineering stress–engineering strain diagram, we define the yield strain as the strain at which coarse slip and fragmentation of lamellar blocks starts. This implies that sliding of junctions in MRs with respect to their initial positions occurs at any elongation ratio, whereas sliding of meso-domains takes place in the post-yield region of deformations only.

Stress–strain relations and kinetic equations for coarse slip of lamellar blocks are developed by using the laws of thermodynamics. These equations are simplified for uniaxial tension of an incompressible medium. The governing equations are determined by 5 adjustable parameters that are found by fitting observations. Fair agreement is demonstrated between the experimental data and the results of numerical simulation both for non-annealed and annealed specimens.

The main result of the study is that the stress–strain curves (up to the necking points) for specimens not subjected to thermal treatment can be fairly well approximated by the constitutive relations where coarse slip and fragmentation of lamellar blocks are not taken into account. In terms of the model, this assertion means that necking of non-annealed samples occurs in the sub-yield region of deformations and precedes their yielding. On the contrary, annealed specimens demonstrate pronounced yield points at relatively small elongation ratios, far below the strains corresponding to the onset of necking.

The following conclusions have been drawn:

1. The elastic modulus, E, monotonically grows with the Hencky strain rate, $\dot{\epsilon}_{\mathrm{H}}$, for non-annealed specimens and monotonically decreases for annealed ones. The difference in the mechanical response of these samples is attributed to a dramatic decrease in the average length of tie strands at thermal treatment.

2. The rate of a developed viscoplastic flow a (that reflects sliding of junctions in amorphous regions and fine slip of crystalline blocks) and the strain ε (that characterizes transition to the steady flow of junctions) increase with the strain rate. These observations are associated with mechanically-induced breakage of tie chains that results in the growth of molecular mobility in amorphous meso-regions.

3. The rate, Γ, of coarse slip and fragmentation of lamellar blocks in the post-yield region of deformations is independent of mechanical factors.

4. The dimensionless parameter η (that characterizes strain-hardening of a semicrystalline polymer above the yield point) grows with the Hencky strain rate. This observation is explained by enhancement of breakage of tie chains with an increase in the rate of straining, and, as a consequence, by an acceleration of alignment of disintegrated lamellar blocks along the direction of longitudinal stress.

References

[1] Brooks NW, Unwin AP, Duckett RA, Ward IM. J Polym Sci B: Polym Phys 1997; 35: 545–552.

[2] Gaucher-Miri V, Seguela R. Macromolecules 1997; 30: 1158–1167.

[3] Brooks NWJ, Duckett RA, Ward IM. J Polym Sci B: Polym Phys 1998; 36: 2177–2189.

[4] Hiss R, Hobeika S, Lynn C, Strobl G. Macromolecules 1999; 32: 4390–4403.

[5] Sabbagh AB, Lesser AJ. J Polym Sci B: Polym Phys 1999; 37: 2651–2663.

[6] Meyer RW, Pruitt LA. Polymer 2001; 42: 5293–5306.

[7] Bergström JS, Kurtz SM, Rimnac CM, Edidin AA. Biomaterials 2002; 23: 2329–2343.

[8] Seguela R. J Polym Sci B: Polym Phys 2002; 40: 593–601.

[9] Sweeney J, Collins TLD, Coates PD, Unwin AP, Duckett RA, Ward IM. Int J Plasticity 2002; 18: 399–414.

[10] Aboulfaraj M, G'Sell C, Ulrich B, Dahoun A. Polymer 1995; 36: 731–742.

[11] Alberola N, Fugier M, Petit D, Fillon B. J Mater Sci 1995; 30: 860–868.

[12] Alberola N, Fugier M, Petit D, Fillon B. J Mater Sci 1995; 30: 1187–1195.

[13] O'Kane WJ, Young RJ. J Mater Sci Lett 1995; 14: 433–435.

[14] O'Kane WJ, Young RJ, Ryan AJ. J Macromol Sci B Phys 1995; 34: 427–458.

[15] Sweeney J, Collins TLD, Coates PD, Ward IM. Polymer 1997; 38: 5991–5999.

[16] Coulon G, Castelein G, G'Sell C. Polymer 1998; 40: 95–110.

[17] Sweeney J, Collins TLD, Coates PD, Duckett RA. J Appl Polym Sci 1999; 72: 563–575.

[18] Seguela R, Staniek E, Escaig B, Fillon B. J Appl Polym Sci 1999; 71: 1873–1885.

[19] Nitta K-H, Takayanagi M. J Polym Sci B: Polym Phys 1999; 37: 357–368.

[20] Nitta K-H, Takayanagi M. J Polym Sci B: Polym Phys 2000; 38: 1037–1044.

[21] Ran S, Zong X, Fang D, Hsia BS, Chu B, Phillips RA. Macromolecules 2001; 34: 2569–2578.

[22] Lima MFS, Vasconcellos MAZ, Samios D. J Polym Sci B: Polym Phys 2002; 40: 896–903.

[23] Buckley CP, Jones DP, Jones DC. Polymer 1996; 37: 2403–2414.

[24] Ajji A, Guevremont J, Cole KC, Dumoulin MM, Polymer 1996; 37: 3707-3714.

[25] Matthews RG, Duckett RA, Ward IM, Jones DP. Polymer 1997; 38: 4795–4802.

[26] Zaroulis JS, Boyce MC. Polymer 1997; 38: 1303–1315.

[27] Adams AM, Buckley CP, Jones DP. Polymer 1998; 39: 5761–5763.

[28] Llana PG, Boyce MC. Polymer 1999; 40: 6729–6751.

[29] Suzuki A, Nakamura Y, Kunugi T. J Polym Sci B: Polym Phys 1999; 37: 1703–1713.

[30] Boyce MC, Socrate S, Llana PG. Polymer 2000; 41: 2183–2201.

[31] Kalay G, Bevis MJ. J Polym Sci B: Polym Phys 1997; 35: 241–263, 265–291.

[32] Yamada K, Matsumoto S, Tagashira K, Hikosaka M. Polymer 1998; 39: 5327–5333.

[33] Alamo RG, Brown GM, Mandelkern L, Lehtinen A, Paukkeri R. Polymer 1999; 40: 3933–3944.

[34] Maiti P, Hikosaka M, Yamada K, Toda A, Gu F. Macromolecules 2000; 33: 9069–9075.

[35] Iijima M, Strobl G. Macromolecules 2000; 33: 5204–5214.

[36] Gu F, Hikosaka M, Toda A, Ghosh SK, Yamazaki S, Araki M, Yamada K. Polymer 2002; 43: 1473–1481.

[37] Meddad A, Fisa B. J Appl Polym Sci 1997; 64: 653–665.

[38] Drozdov AD, Christiansen JdeC. Polymer 2002; 43: 4745–4761.

[39] Quinson R, Perez J, Rink M, Pavan A. J Mater Sci 1997; 32: 1371–1379.

[40] Haupt P. Continuum mechanics and theory of materials, Berlin: Springer, 2000.

[41] Kloczkowski A. Polymer 2002; 43: 1503–1525.

[42] Drozdov AD, Christiansen JdeC. Eur Polym J 2002; 38: in press.

[43] Kaye A, Kennett AJ. Rheol Acta 1974; 13: 916–923.

[44] Hasan OA, Boyce MC. Polym Eng Sci 1995; 35: 331–344.

[45] Bordonaro CM, Krempl E. Polym Eng Sci 1995; 35: 310–316.

[46] Bardenhagen SG, Stout MG, Gray GT. Mech Mater 1997; 25: 235–253.

[47] Spathis G, Kontou E. Polymer 1998; 39: 135–142.

[48] Frank GJ, Brockman RA. Int J Solids Structures 2001; 38: 5149–5164.

[49] Jolly L, Tidu A, Heizmann I-J, Bolle B. Polymer 2002; 43: in press.

List of figures

Figure 1: The true stress Σ MPa versus the elongation ratio k in a tensile test with the cross-head speed 5 mm/min. Circles: experimental data for a non-annealed specimen. Vector indicates the beginning of necking. Solid line: results of numerical simulation

Figure 2: The true stress Σ MPa versus the elongation ratio k in a tensile test with the cross-head speed 10 mm/min. Circles: experimental data for a non-annealed specimen. Vector indicates the beginning of necking. Solid line: results of numerical simulation

Figure 3: The true stress Σ MPa versus the elongation ratio k in a tensile test with the cross-head speed 25 mm/min. Circles: experimental data for a non-annealed specimen. Vector indicates the beginning of necking. Solid line: results of numerical simulation

Figure 4: The true stress Σ MPa versus the elongation ratio k in a tensile test with the cross-head speed 50 mm/min. Circles: experimental data for a non-annealed specimen. Vector indicates the beginning of necking. Solid line: results of numerical simulation

Figure 5: The true stress Σ MPa versus the elongation ratio k in a tensile test with the cross-head speed 100 mm/min. Circles: experimental data for a non-annealed specimen. Solid line: results of numerical simulation

Figure 6: The true stress Σ MPa versus the elongation ratio k in a tensile test with the cross-head speed 150 mm/min. Circles: experimental data for a non-annealed specimen. Vector indicates the beginning of necking. Solid line: results of numerical simulation

Figure 7: The true stress Σ MPa versus the elongation ratio k in a tensile test with the cross-head speed 200 mm/min. Circles: experimental data for a non-annealed specimen. Vector indicates the beginning of necking. Solid line: results of numerical simulation

Figure 8: The true stress Σ MPa versus the elongation ratio k in a tensile test with the cross-head speed 5 mm/min. Circles: experimental data for an annealed specimen. Solid line: results of numerical simulation

Figure 9: The true stress Σ MPa versus the elongation ratio k in a tensile test with the cross-head speed 10 mm/min. Circles: experimental data for an annealed specimen. Solid line: results of numerical simulation

Figure 10: The true stress Σ MPa versus the elongation ratio k in a tensile test with the cross-head speed 25 mm/min. Circles: experimental data for an annealed specimen. Solid line: results of numerical simulation

Figure 11: The true stress Σ MPa versus the elongation ratio k in a tensile test with the cross-head speed 50 mm/min. Circles: experimental data for an annealed specimen. Solid line: results of numerical simulation

Figure 12: The true stress Σ MPa versus the elongation ratio k in a tensile test with the cross-head speed 100 mm/min. Circles: experimental data for an annealed specimen. Solid line: results of numerical simulation

Figure 13: The true stress Σ MPa versus the elongation ratio k in a tensile test with the cross-head speed 150 mm/min. Circles: experimental data for an annealed specimen. Solid

line: results of numerical simulation

Figure 14: The true stress Σ MPa versus the elongation ratio k in a tensile test with the cross-head speed 200 mm/min. Circles: experimental data for an annealed specimen. Vector indicates the beginning of necking. Solid line: results of numerical simulation

Figure 15: The true yield stress Σ_y MPa (unfilled circles) and the elongation ratio for yielding k_y (filled circles) versus the strain rate $\dot{\epsilon}_H$ s^{-1}. Symbols: treatment of observations. Solid lines: approximation of the experimental data by Eq. (1) with $\Sigma_0 = 39.27$ and $\Sigma_1 = 2.32$ (curve 1) and by the constant $k_y = 1.0473$ (curve 2)

Figure 16: The elastic modulus E GPa versus the strain rate $\dot{\epsilon}_H$ s^{-1}. Symbols: treatment of observations. Unfilled circles: non-annealed specimens; filled circles: annealed specimens. Solid lines: approximation of the experimental data by Eq. (63). Curve 1: $E_0 = 0.81$, $E_1 = 0.07$; curve 2: $E_0 = 0.43$, $E_1 = -0.22$

Figure 17: The dimensionless rate a of a developed flow of junctions versus the strain rate $\dot{\epsilon}_H$ s^{-1}. Symbols: treatment of observations. Unfilled circles: non-annealed specimens; filled circles: annealed specimens. Solid lines: approximation of the experimental data by Eq. (63). Curve 1: $a_0 = 0.93$, $a_1 = 0.033$; curve 2: $a_0 = 0.82$, $a_1 = 0.042$

Figure 18: The strain ε that characterizes transition to a developed flow of junctions versus the strain rate $\dot{\epsilon}_H$ s^{-1}. Symbols: treatment of observations. Unfilled circles: non-annealed specimens; filled circles: annealed specimens. Solid lines: approximation of the experimental data by Eq. (63). Curve 1: $\varepsilon_0 = -1.15$, $\varepsilon_1 = 0.028$; curve 2: $\varepsilon_0 = -0.62$, $\varepsilon_1 = 0.375$

Figure 19: The dimensionless rate of coarse slip of lamellar blocks Γ versus the strain rate $\dot{\epsilon}_H$ s^{-1}. Circles: treatment of observations for annealed specimens. Solid line: approximation of the experimental data by the constant $\Gamma_0 = 6.07$

Figure 20: The dimensionless parameter η that characterizes strain-hardening versus the strain rate $\dot{\epsilon}_H$ s^{-1}. Circles: treatment of observations for annealed specimens. Solid line: approximation of the experimental data by Eq. (64) with $\eta_0 = 0.0328$ and $\eta_1 = 0.0072$
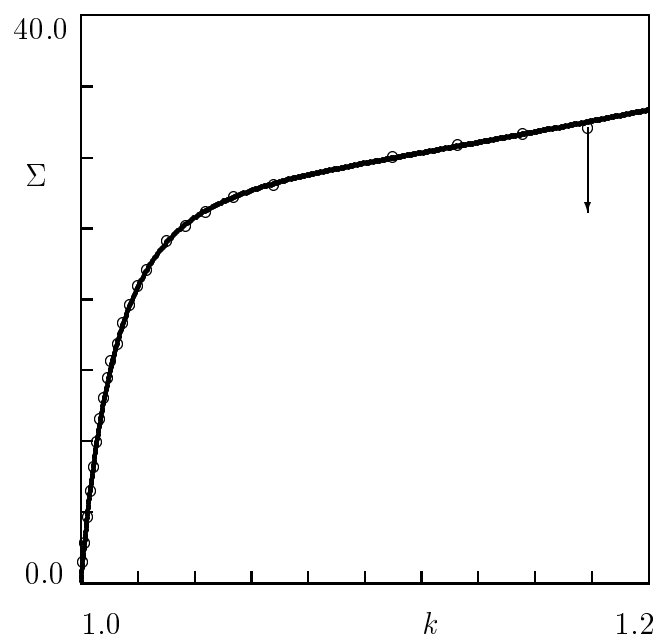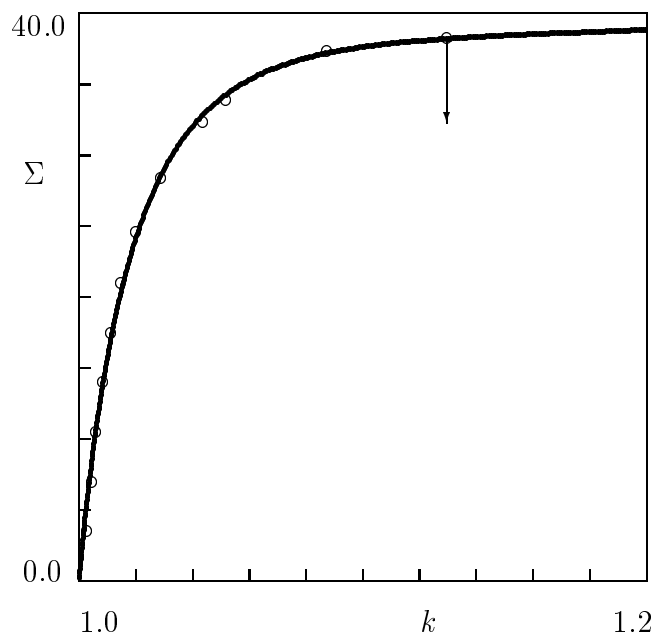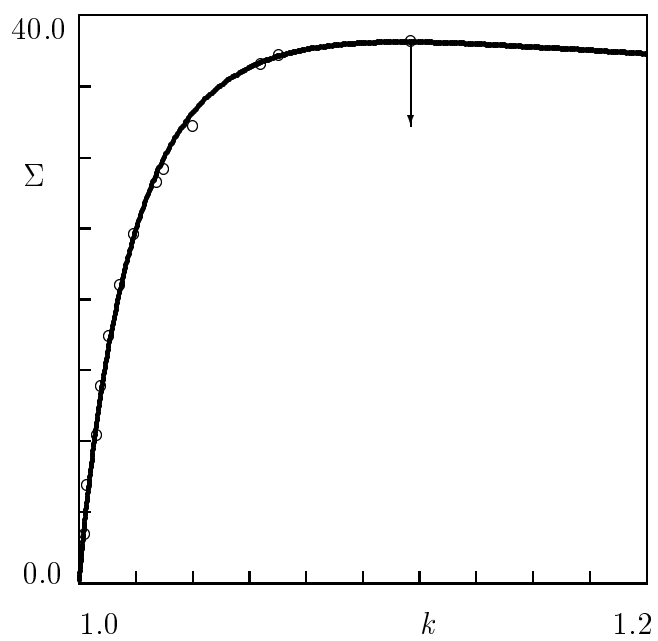
Figure 1:
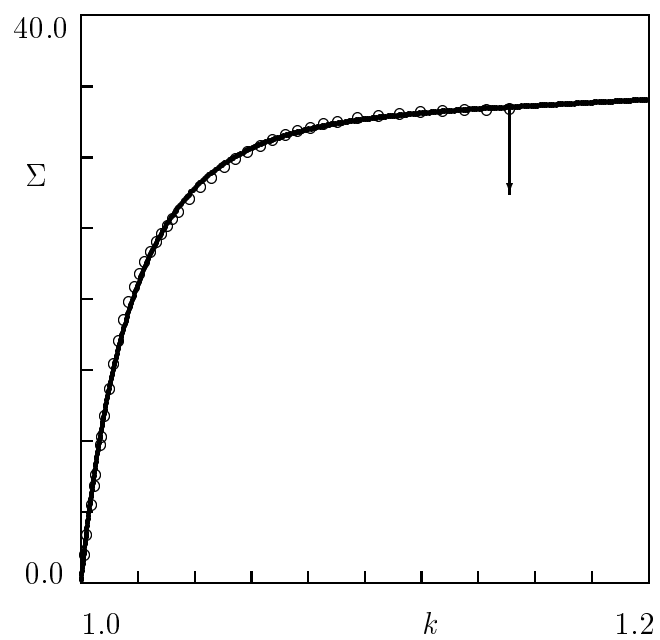
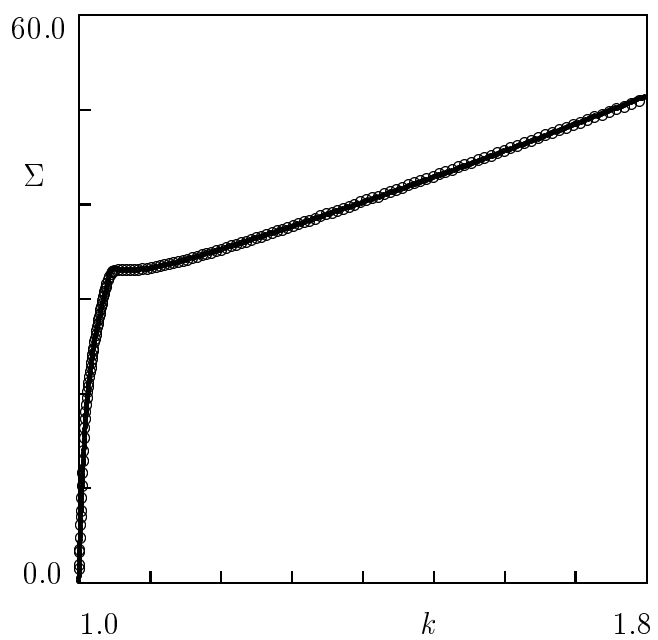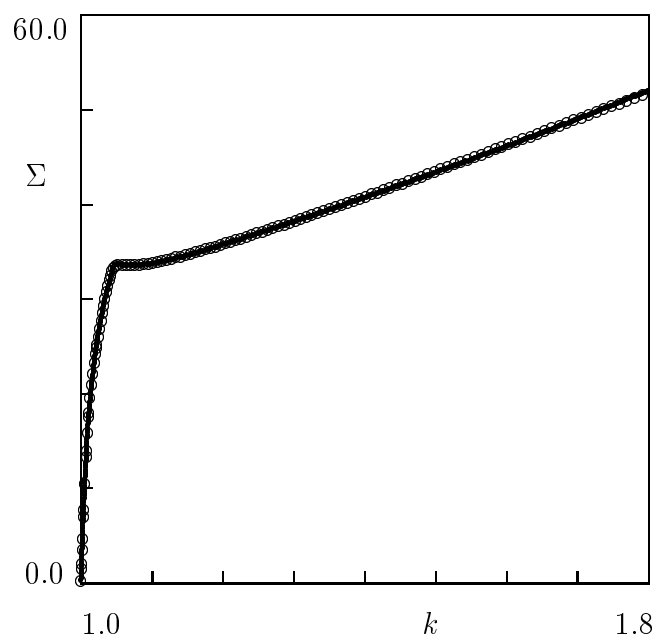Figure 2:
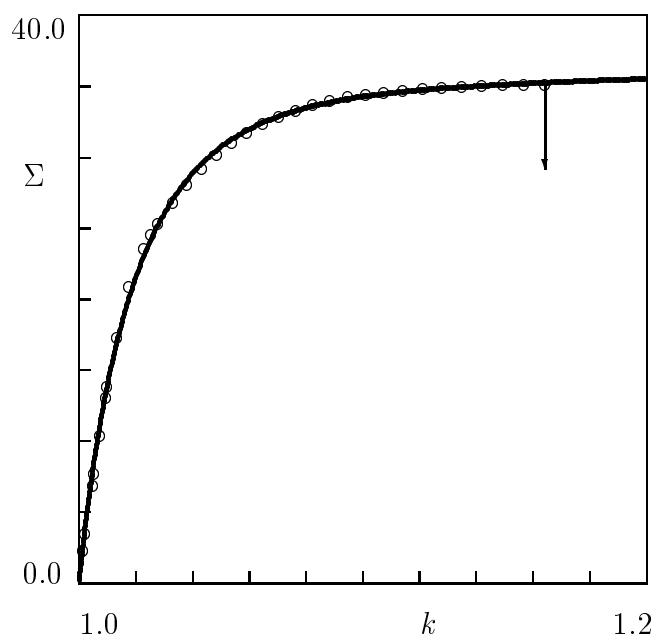
Figure 3:
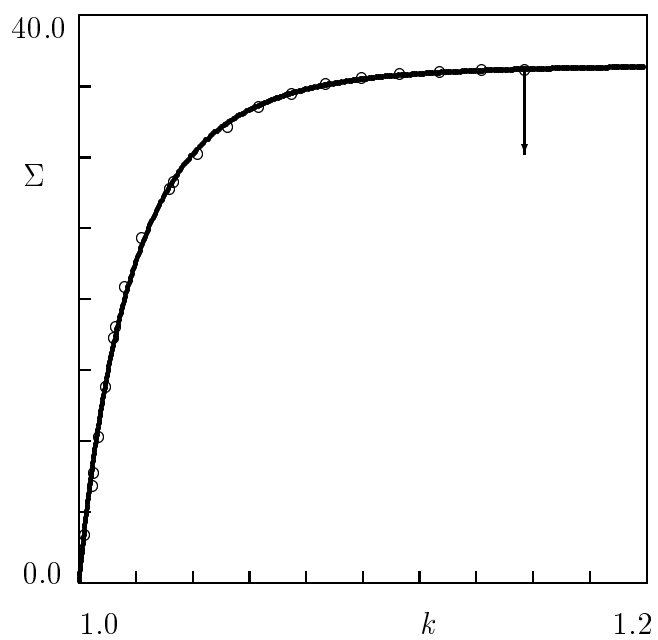
Figure 4:
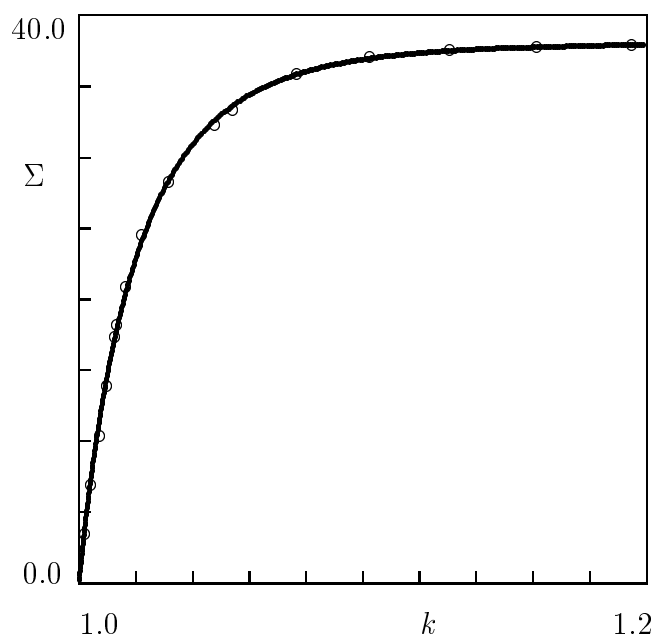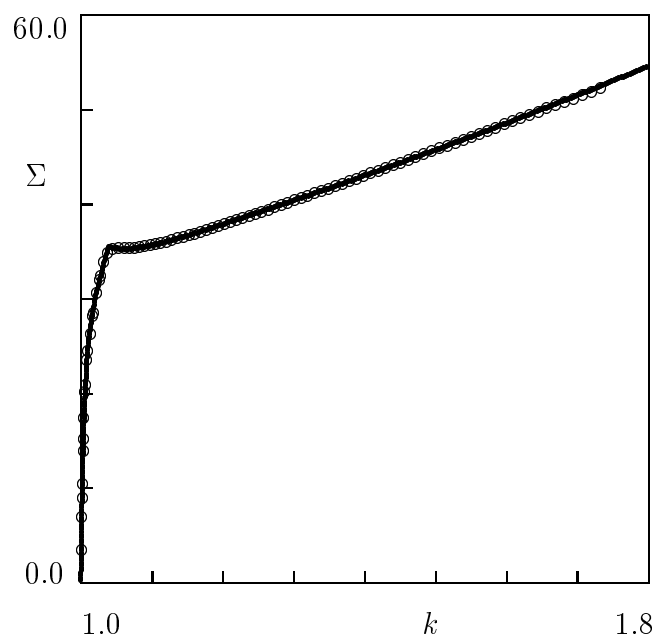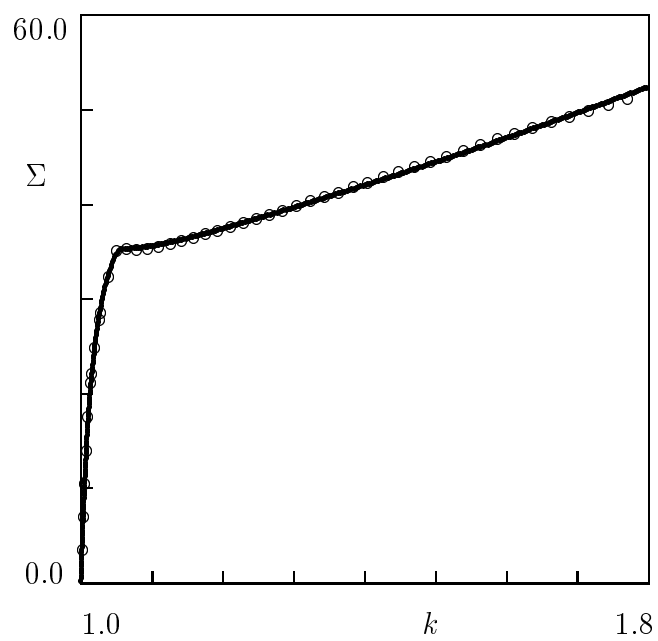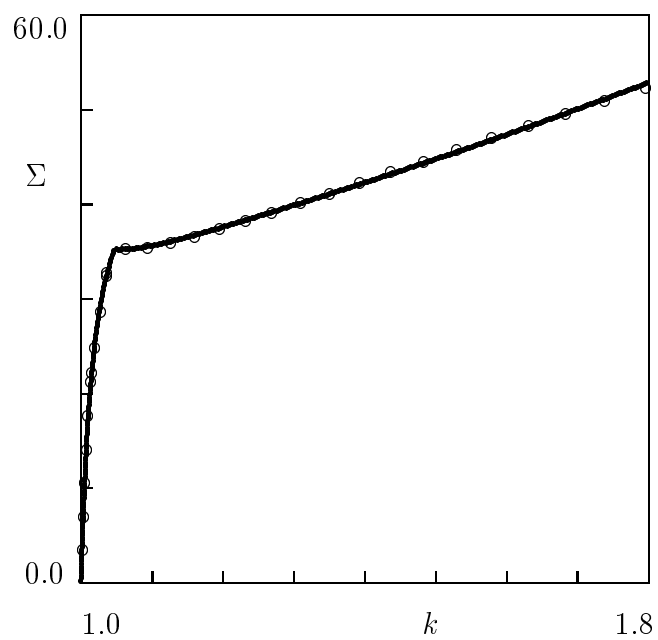
Figure 5:

Figure 6:

Figure 7:
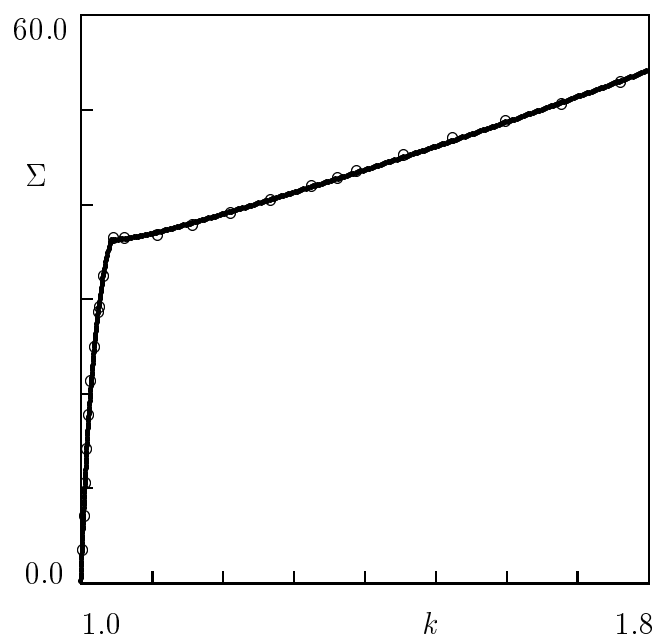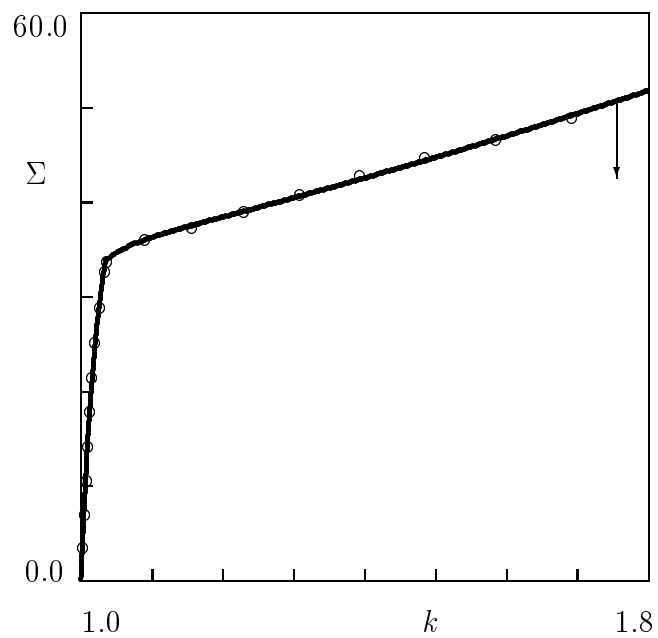

Figure 8:

Figure 9:

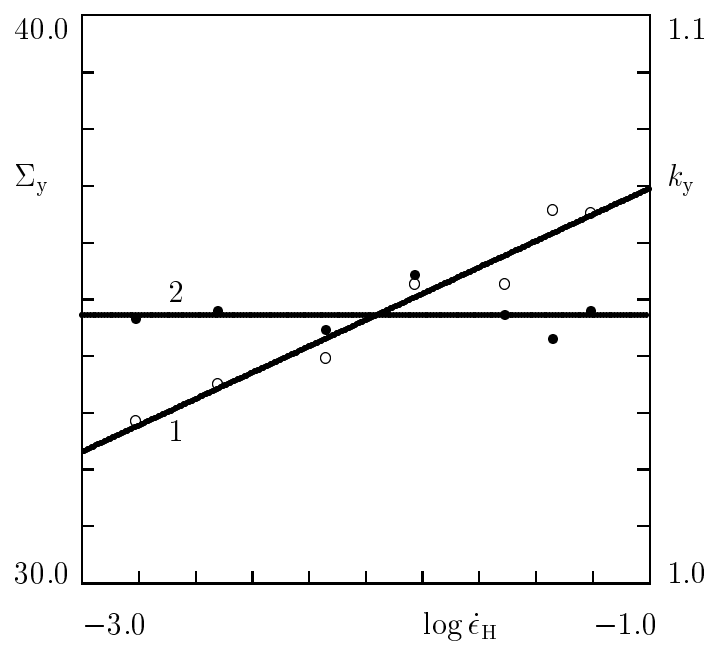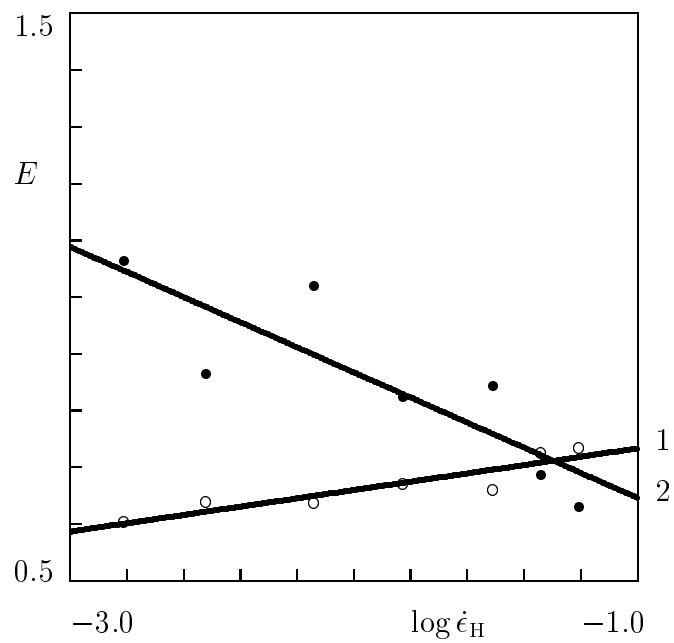

Figure 10:

Figure 11:

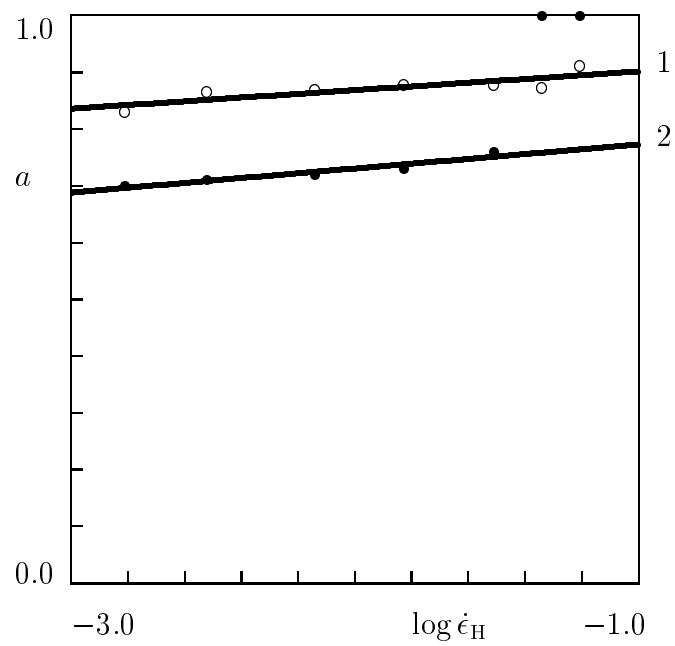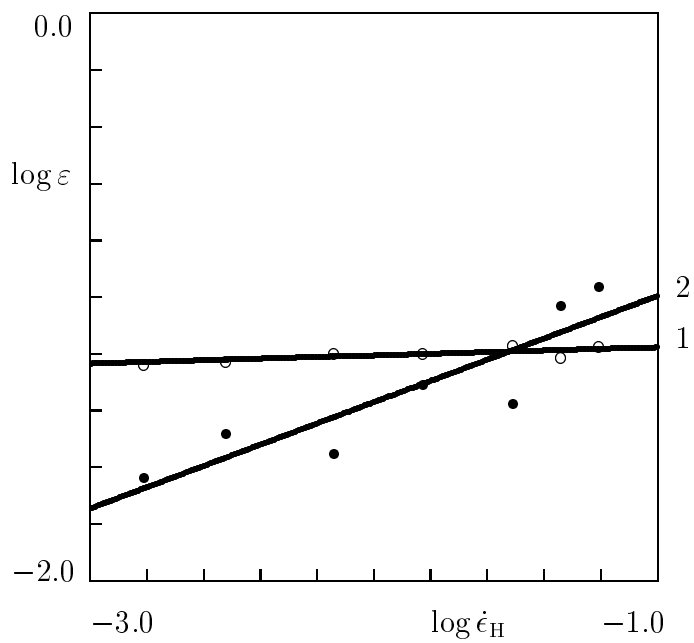Figure 12:

Figure 13:

Figure 14:

Figure 15:

Figure 16:

Figure 17:

Figure 18:

Figure 19:

Figure 20: